

# Probing CP Violation and Mass Hierarchy in Neutrino Oscillations in Matter through Quantum Speed Limits

Subhadip Bouri<sup>1,\*</sup>, Abhishek Kumar Jha<sup>1,†</sup> and Subhashish Banerjee<sup>2,‡</sup>

<sup>1</sup>*Department of Physics, Indian Institute of Science, Bangalore 560012, India*

<sup>2</sup>*Indian Institute of Technology Jodhpur, Jodhpur 342011, India*

(Dated: May 24, 2024)

The quantum speed limits (QSLs) set fundamental lower bounds on the time required for a quantum system to evolve from a given initial state to a final state. In this work, we investigate CP violation and the mass hierarchy problem of neutrino oscillations in matter using the QSL time as a key analytical tool. We examine the QSL time for the unitary evolution of two- and three-flavor neutrino states, both in vacuum and in the presence of matter. Two-flavor neutrino oscillations are used as a precursor to their three-flavor counterparts. We further compute the QSL time for neutrino state evolution and entanglement in terms of neutrino survival and oscillation probabilities, which are experimentally measurable quantities in neutrino experiments. A difference in the QSL time between the normal and inverted mass hierarchy scenarios, for neutrino state evolution as well as for entanglement, under the effect of a CP violation phase is observed. Our results are illustrated using energy-varying sets of accelerator neutrino sources from experiments such as T2K, NOvA, and DUNE. Notably, three-flavor neutrino oscillations in constant matter density exhibit faster state evolution across all these neutrino experiments in the normal mass hierarchy scenario. Additionally, we observe fast entanglement growth in DUNE assuming a normal mass hierarchy.

## I. INTRODUCTION

The uncertainty relations are widely regarded as a fundamental aspect of modern physics, representing the uncertainty relationship between conjugate variables in a quantum mechanical system [1, 2]. Mandelstam and Tamm (MT) demonstrated that the energy, time uncertainty relation can be understood as imposing limits on the evolution rate of a quantum system [3]. Another bound on the quantum evolution time was subsequently obtained by Margolus and Levitin (ML) in terms of the initial mean energy of the quantum system [4]. Both MT and ML were combined to provide a tight bound on the minimum time required for a quantum system to evolve from an initial state to the final state under a given dynamical process [5]. The limit arises due to the intrinsic dynamical timescales of a quantum system. This limitation on a quantum system's evolution time is known as the quantum speed limit (QSL) time. Over the last decade, by employing the geometric approach, the topic of QSL time has been extensively researched [6–12]. In Ref. [11], the QSL time was shown to provide the fundamental limit on the rate of evolution of closed quantum systems, whose dynamics is unitary. The Bures angle can be considered a measure of the “closeness” between the initial and final states of the evolved quantum system. The QSL time for the evolution of a quantum system through the state space can be expressed as a function of the Bures angle and is inversely proportional to the variance of the driving Hamiltonian. Moreover, the generalization of QSL time has been explored for driven closed [13] and open quantum systems [14, 15]. The QSL time has broad applications in various quantum tasks, such as quantum information [16–20], quantum correlations [21], quantum computation [22], quantum

metrology [23, 24], non-equilibrium quantum entropy production [14], quantum thermodynamics [25, 26], quantum optimal control algorithms [27, 28], quantum batteries [29–32] and quantum gravity [33–36]. In recent times, in the realm of particle physics, the impact of open quantum system and information theoretic ideas, such as, the QSL time, has been made on the neutral meson [37–39] and the neutrino system [40].

Neutrinos are weakly interacting particles with nonzero mass [41], as demonstrated by experiments with atmospheric [42, 43] and solar neutrinos [44]. It is known that a neutrino of a specific flavor  $\nu_\alpha$  (where  $\alpha \in e, \mu, \tau$ ) undergoes time evolution and may be detected in a distinct flavor state [45–50]. This phenomenon constitutes the essence of neutrino oscillations. Flavor oscillations occur because neutrinos exist as a mixture of different masses. A flavor state can be written as a linear superposition of three non-degenerate mass-eigenstates. Both flavor and mass eigenstates can be related by the unitary transformation matrix known as Pontecorvo-Maki-Nakagawa-Sakata (PMNS) mixing matrix [51]. In the standard three-flavor neutrino oscillations in vacuum, the PMNS matrix of Dirac neutrinos is fully described by three mixing angles  $\theta_{12}$ ,  $\theta_{23}$ , and  $\theta_{13}$  and a complex phase  $\delta_{CP}$  related to charge-conjugation and parity-reversal (CP) symmetry violations [50]. The survival and oscillation probabilities of initial neutrino flavor states can be related to the three mixing angles, two squared-mass differences and the ratio of Length to Energy ( $L/E$ ), where  $L$  is the distance between the neutrino source and detector, and  $E$  is the neutrino source energy. Parameters linked to these probabilities are measurable in neutrino experiments. The quest to investigate precise measurements of PMNS mixing parameters [50], CP-violation phases [52–54], and other issues such as neutrino mass hierarchy (whether the neutrino mass ordering is normal or inverted in nature) [55], sterile neutrinos, are the primary focus of the current neutrino experiments including solar [56], atmosphere [57], reactor (Short- and Long-Baseline) [58–60], and accel-

\* subhadipb@iisc.ac.in

† kjabhishek@iisc.ac.in

‡ subhashish@iitj.ac.in

erator (Long-Baseline) [61, 62].

In a close quantum system, the dynamical evolution of the neutrino system is governed by unitary transformation. The driving Hamiltonian for neutrino flavor oscillations in the presence of earth's matter background is the effective Hamiltonian [63–67], which can be described by two regions of neutrino state propagation: in vacuum and in the presence of constant matter. Thus, a natural question arises: how quickly does the neutrino flavor state change with time in these two regions of propagation? In this paper, we aim to answer this question by examining in detail the QSL time for the unitary dynamics of two- and three-flavor neutrino oscillations in matter. In this context, we quantify the Bures angle in relation to neutrino survival probability, providing insight into the proximity between the initial and final states of time-evolved flavor neutrino states in vacuum and in a constant matter background. Furthermore, we compute the variance in the driving Hamiltonian for various regions of neutrino flavor state propagation with time. The study of QSL time in two-flavor neutrino oscillations in matter serves as a precursor to understanding three-flavor neutrino oscillations, actually occurring in nature. In three-flavor neutrino oscillations, considering matter effects and CP violation, we discuss the behavior of the QSL time for ongoing accelerator Long-Baseline neutrino source experiments like NOvA and T2K, as well as for the upcoming experiment DUNE. Further, we analyze the QSL time for the initial muon neutrino and muon anti-neutrino flavor states. Our analysis reveals that the QSL time demonstrates sensitivity to the normal and inverted mass-hierarchy scenarios and CP violation in neutrino physics.

Furthermore, quantum entanglement and coherence are two fundamental features arising from the principle of quantum superposition [68]. Since the time-evolved neutrino state is a coherent superposition state, it is natural to study quantum entanglement in the neutrino system. In the plane-wave framework of two and three-flavor neutrino oscillations, the linear superposition of neutrino states have been mapped to two- and three-mode quantum states, representing two- and three-qubit Bell's type states, respectively [69–88]. It is known that the concept of entanglement play a crucial role in quantifying and characterizing entanglement in the time-evolved neutrino mode (flavor) state. Various multi-mode entanglement measures, such as concurrence, linear entropy, teleportation fidelity, geometric discord, von Neumann entropy, tangle, negativity, three-tangle, three- $\pi$ , have been quantified in terms of neutrino flavor transition probabilities. Also, other aspects like Bell's inequality and Bell-CHSH (Clauser-Horn-Shimony-Holt) inequality violations have been studied in the context of neutrino oscillations [69–88]. As a three-qubit system, the three-flavor neutrino states resemble the generalized W-states [79]. Additionally, the study of the mode-entanglement using the wave-packet approach in neutrino oscillations has been done [89–93]. These suggest that genuine multipartite entanglement persists in the neutrino flavor-changing states. Moreover, the nonclassical nature of neutrino oscillations was investigated using temporal analogues of Bell inequalities, such as Leggett-Garg inequalities (LGI) [94–101]. Quantum coherence in neutrino oscillations can be maintained

over a long distance and observed in different experiments [102–104]. Furthermore, by encoding neutrinos in a multi-qubit system, potential use of neutrino oscillations has been made for quantum computation as well [105–108].

The study of the QSL time for quantum evolution has unveiled fundamental constraints on the rate of change of various entanglement measures [109–111]. Specifically, QSL time for entanglement entropy has been investigated for the bi-partite pure quantum system [112]. The simplest case of a multi-partite quantum system is a bi-partite quantum system comprising two subsystems. Entanglement entropy serves as an important entanglement measure to assess the degree of quantum entanglement between the subsystems of a bi-partite quantum system. The entanglement entropy determines the von Neumann entropy on the reduced density matrix of one of the subsystems [113]. It quantifies the uncertainty resulting from the lack of a well-defined quantum state in a subsystem due to potential entanglement with another subsystem. The variance in entanglement entropy is defined as the capacity of entanglement of the reduced state of any of the subsystems [114, 115]. The QSL time for entanglement entropy shown in Ref. [112] estimates how fast entanglement may be formed or degraded in a bi-partite quantum system.

Recently, to probe the astrophysical neutrinos, bipartite entanglement entropy has been proposed to quantify entanglement in quantum many-body collective neutrino flavor oscillations [116–118]. However, in this work, we consider a single-particle neutrino system as a bi-partite quantum system. By mapping the two-flavour neutrino state to the two-qubit state, we quantify the entanglement entropy and the capacity of entanglement in two-flavor neutrino oscillations in vacuum and in the presence of constant earth-matter background. Furthermore, we extend our investigation to study the fundamental limit on the time required for entanglement entropy in three-flavor neutrino oscillations with CP-violation phase, considering normal and inverted mass hierarchy scenarios. We use Long-Baseline accelerator neutrino source data from T2K, NOvA, and DUNE experiments, corresponding to distinct energies to characterize our results.

The organization of the paper is as follows: In Sect. II, we briefly review the QSL time for quantum evolution and for entanglement. In Sect. III, the quantum phenomena of the three-flavor neutrino oscillation is described in vacuum and in constant earth-matter backgrounds. In Sect. IV, the QSL time is computed in two-flavor scenarios, especially for the time evolution of electron-flavor neutrino states propagating in vacuum and in presence of a constant earth-matter potential. Moreover, we map neutrinos to two-qubit states and explore various bi-partite entanglement measures such as entanglement entropy and capacity of entanglement. In Sect. V, we explore the QSL time for the initial muon neutrino and muon anti-neutrino flavor states evolving in matter in the presence of CP-violation phase, and under the assumptions of normal and inverted mass hierarchy. Furthermore, in Sect. VI, we map the initial muon flavor neutrino state to a three-qubit state and investigate various bi-partite entanglement measures such as entanglement entropy and capacity of entanglement as the initial muon flavor neutrino propagates in space with a con-

stant earth-matter background. We estimate the QSL time for entanglement entropy in the presence of matter and the CP-violation phase, considering normal and inverted mass hierarchy. Discussions and conclusions are made in Sect. VII.

## II. QUANTUM SPEED LIMIT TIME FOR QUANTUM EVOLUTION AND FOR ENTANGLEMENT

In quantum mechanics, the state of a quantum system is described by a wave function  $|\psi\rangle$ , and the time evolution of this wave function is given by the Schrödinger equation [68]

$$i\hbar \frac{d|\psi\rangle}{dt} = \mathcal{H}|\psi\rangle \implies |\psi_\tau\rangle = e^{-i\mathcal{H}\tau/\hbar} |\psi_0\rangle \equiv U_\tau |\psi_0\rangle, \quad (1)$$

where  $U_\tau$  is the unitary time evolution operator ( $U_\tau U_\tau^\dagger = I$ ). An initial pure state remains pure due to the unitary dynamics. In this case, the initial and final states can be represented in density matrix form as  $\rho_0 = |\psi_0\rangle\langle\psi_0|$ , and  $\rho_\tau = |\psi_\tau\rangle\langle\psi_\tau|$ , respectively. The driving Hamiltonian  $\mathcal{H}$  for the initial pure state  $\rho_0$  can be either time-independent or time-dependent, and is Hermitian  $\mathcal{H}^\dagger = \mathcal{H}$ .

MT and ML-type bounds on speed limit time are estimated by using geometrical approaches to quantify the closeness between the initial and final states [12]. Here, the Bures angle is employed to measure the distance between two quantum states

$$\mathcal{B} = \cos^{-1} \sqrt{\mathcal{F}(\psi_0, \psi_\tau)}. \quad (2)$$

In eqn. (2),  $\mathcal{F} = \text{Tr}(\rho_0\rho_\tau) = |\langle\psi_0|\psi_\tau\rangle|^2$  represent the survival probability of the initial pure state  $\rho_0$  and is known as fidelity.  $\mathcal{F} = 1$ , implies that  $\rho_\tau$  is same as  $\rho_0$ . For the initial pure state  $\rho_0$ , the time-independent QSL time is defined by [11]

$$\tau \geq \tau_{\text{QSL}} = \frac{4\hbar}{\pi^2 E_\tau} \mathcal{B}^2(\psi_0, \psi_\tau), \quad (3)$$

where

$$E_\tau = 1/\tau \int_0^\tau dt |\langle\psi_t | \mathcal{H} | \psi_t\rangle| \quad (4)$$

is the time-averaged mean energy.

Furthermore, in a bi-partite pure quantum system, a state of the quantum system can be represented as the tensor product of minimum two-qubit Hilbert spaces [68]:  $|\psi\rangle \in H_A \otimes H_B$ . For example, a two-qubit Bell-type superposition state can be considered as a bi-partite quantum state:  $|\psi\rangle = \alpha|10\rangle + \beta|01\rangle$ ,  $|\alpha|^2 + |\beta|^2 = 1$ , where,  $|01\rangle = |0\rangle \otimes |1\rangle$  and  $|10\rangle = |1\rangle \otimes |0\rangle$  are two-qubit basis states of  $|\psi\rangle$ . In general, Bell's state of two-qubit or more than two-qubit representation can be regarded as a bi-partite pure entangled state. Any entangled bi-partite pure quantum system  $\rho_{AB} = |\psi\rangle\langle\psi|$  consists of two sub-systems  $\rho_A = \text{Tr}_B(\rho_{AB})$  and  $\rho_B = \text{Tr}_A(\rho_{AB})$  such that  $\rho \neq \rho_A \otimes \rho_B$ , where  $\rho_A$  and  $\rho_B$  are two reduced density matrices. The entanglement entropy  $S_{EE}$  for  $\rho_A$  (or  $\rho_B$ ) is defined as [113]

$$S_{EE} = S(\rho_A) = -\text{Tr}(\rho_A \log_2 \rho_A). \quad (5)$$

Moreover, if the dynamics of the system is unitary and the driving Hamiltonian remains time-independent, the quantum speed limit for the entanglement entropy ( $S_{EE}$ ) adheres to the following bound [112]

$$\tau \geq \tau_{\text{QSL}}^E = \frac{\hbar |S_{EE}(\tau) - S_{EE}(0)|}{2\Delta\mathcal{H} \frac{1}{\tau} \int_0^\tau \sqrt{C_E(t)} dt}, \quad (6)$$

where  $\Delta\mathcal{H} = \sqrt{\langle\mathcal{H}^2\rangle - \langle\mathcal{H}\rangle^2}$  is the variance (or fluctuation) in the driving Hamiltonian ( $\mathcal{H}$ ). The variance in the entanglement entropy  $S_{EE}$  is defined as capacity of entanglement  $C_E$  [114, 115], and is

$$C_E = \sum_i \lambda_i \log_2^2 \lambda_i - S_{EE}^2. \quad (7)$$

Here,  $\lambda_i$ 's are the eigenvalue of the reduced density matrix  $\rho_A$  of one of the subsystems of a given pure bipartite quantum system  $\rho_{AB}$ , where  $\text{Tr}(\rho_{AB}^2) = 1$  and  $\text{Tr}(\rho_A^2) < 1$ . Equation (6) establishes a quantum speed limit on the production and decay of entanglement in the case of pure bipartite states when the driving Hamiltonian is time-independent.

## III. EVOLUTION OF THREE-FLAVOR NEUTRINO OSCILLATIONS

Here we provide a brief introduction to three flavour neutrino oscillations in vacuum as well as in matter.

### A. Oscillations in vacuum

In the plane-wave approximation of the three-flavor neutrino oscillation in vacuum, the neutrino flavor states  $|\nu_\alpha\rangle$  ( $\alpha = e, \mu, \tau$ ) are linear superposition of mass eigenstates  $|\nu_j\rangle$  ( $j = 1, 2, 3$ ):  $|\nu_\alpha\rangle = \sum_j U_{\alpha j}^* |\nu_j\rangle$ , where the asterisk denotes the complex conjugation of  $U_{\alpha j}$  and are the elements of the lepton mixing matrix known as PMNS matrix such that [41, 50]

$$\begin{pmatrix} |\nu_e\rangle \\ |\nu_\mu\rangle \\ |\nu_\tau\rangle \end{pmatrix} = \begin{pmatrix} U_{e1}^* & U_{e2}^* & U_{e3}^* \\ U_{\mu1}^* & U_{\mu2}^* & U_{\mu3}^* \\ U_{\tau1}^* & U_{\tau2}^* & U_{\tau3}^* \end{pmatrix} \begin{pmatrix} |\nu_1\rangle \\ |\nu_2\rangle \\ |\nu_3\rangle \end{pmatrix}, \quad (8)$$

and  $U_{\text{PMNS}}(\theta_{ij}, \delta_{\text{CP}}) =$

$$\begin{pmatrix} c_{12}c_{13} & s_{12}c_{13} & s_{13}e^{-i\delta_{\text{CP}}} \\ -s_{12}c_{23} - c_{12}s_{23}s_{13}e^{i\delta_{\text{CP}}} & c_{12}c_{23} - s_{12}s_{23}s_{13}e^{i\delta_{\text{CP}}} & s_{23}c_{13} \\ s_{12}s_{23} - c_{12}c_{23}s_{13}e^{i\delta_{\text{CP}}} & -c_{12}s_{23} - s_{12}c_{23}s_{13}e^{i\delta_{\text{CP}}} & c_{23}c_{13} \end{pmatrix}, \quad (9)$$

with  $c_{ij} = \cos(\theta_{ij})$  and  $s_{ij} = \sin(\theta_{ij})$  and  $\delta_{\text{CP}}$  being the CP-violating phase. In light of recent experiments, the phase  $\delta_{\text{CP}}$  is found to potentially hold non-zero values, underscoring the imperative for a re-evaluation of fundamental aspects across virtually all scales within the universe. The evolution equation of the neutrino flavor state  $\nu_\alpha$  in vacuum is governed by the following Schrodinger equation:

$$i \frac{d}{dt} |\nu_\alpha\rangle = \mathcal{H}_{\text{vac}} |\nu_\alpha\rangle, \quad (10)$$

where  $\mathcal{H}_{vac} = \mathcal{H}_{\mathcal{KE}}$  is the Hamiltonian in vacuum, which can be diagonalized by orthogonal transformation as

$$\mathcal{H}_{vac} = \frac{1}{2E} \left( U_{\text{PMNS}} \mathbb{M}^2 U_{\text{PMNS}}^\dagger \right), \quad (11)$$

and

$$\nu_\alpha = \begin{pmatrix} \nu_e \\ \nu_\mu \\ \nu_\tau \end{pmatrix}, \quad \mathbb{M}^2 = \begin{pmatrix} 0 & 0 & 0 \\ 0 & \Delta m_{21}^2 & 0 \\ 0 & 0 & \Delta m_{31}^2 \end{pmatrix}, \quad (12)$$

where  $\Delta m_{21}^2, \Delta m_{31}^2$  are two squared-mass differences in vacuum,  $U_{\text{PMNS}} U_{\text{PMNS}}^\dagger = I$  and  $\mathcal{H}_{vac}^\dagger = \mathcal{H}_{vac}$ . In general, the time-evolved flavor neutrino states in linear superposition of mass basis can be written as  $|\nu_\alpha(t)\rangle = \sum_j U_{\alpha j}^* e^{-im_j^2 \frac{t}{2E}} |\nu_j\rangle$ . Furthermore,  $|\nu_j\rangle = \sum_\beta U_{\beta j} |\nu_\beta\rangle$ , where  $\beta = e, \mu, \tau$ . Using eqn. (8), the time-evolved neutrino flavor state  $|\nu_\alpha(t)\rangle$  in vacuum for an arbitrary initial state  $|\nu_\alpha(0)\rangle = \sum U_{\alpha j}^* |\nu_j(0)\rangle$  can be written in the matrix form as

$$\begin{aligned} |\nu_\alpha(t)\rangle &= e^{-i\mathcal{H}_{vac}t} |\nu_\alpha(0)\rangle \\ &= U_{\text{PMNS}} \Lambda(t) U_{\text{PMNS}}^\dagger |\nu_\alpha(0)\rangle \\ &= U_{\text{PMNS}} \begin{pmatrix} 1 & 0 & 0 \\ 0 & e^{-i\Delta m_{21}^2 \frac{t}{2E}} & 0 \\ 0 & 0 & e^{-i\Delta m_{31}^2 \frac{t}{2E}} \end{pmatrix} U_{\text{PMNS}}^\dagger |\nu_\alpha(0)\rangle \\ &= \begin{pmatrix} \tilde{U}_{ee}(t) & \tilde{U}_{e\mu}(t) & \tilde{U}_{e\tau}(t) \\ \tilde{U}_{\mu e}(t) & \tilde{U}_{\mu\mu}(t) & \tilde{U}_{\mu\tau}(t) \\ \tilde{U}_{\tau e}(t) & \tilde{U}_{\tau\mu}(t) & \tilde{U}_{\tau\tau}(t) \end{pmatrix} |\nu_\alpha(0)\rangle, \end{aligned} \quad (13)$$

where  $E$  as the neutrino energy. Thus, from eqn. (13), the time-evolved neutrino flavor state  $|\nu_\alpha(t)\rangle$  in a linear superposition of flavor basis can be explicitly re-expressed as

$$|\nu_\alpha(t)\rangle = \tilde{U}_{\alpha e}(t) |\nu_e\rangle + \tilde{U}_{\alpha\mu}(t) |\nu_\mu\rangle + \tilde{U}_{\alpha\tau}(t) |\nu_\tau\rangle, \quad (14)$$

where  $|\tilde{U}_{\alpha e}(t)|^2 + |\tilde{U}_{\alpha\mu}(t)|^2 + |\tilde{U}_{\alpha\tau}(t)|^2 = 1$  and  $\tilde{U}_{\alpha\beta}(t) \equiv \sum_j U_{\alpha j}^* e^{-im_j^2 \frac{t}{2E}} U_{\beta j}$ . Since neutrinos are ultra-relativistic particles,  $t \approx L$  (with  $c = 1$  being the speed of light) is the distance traveled by the neutrino. The oscillation probability  $P_O$  that a neutrino originally in flavor  $\alpha$  will later be observed in flavor  $\beta$  is [50]

$$P_O = P_{\alpha \rightarrow \beta} = \left| \langle \nu_\beta(L) | \nu_\alpha \rangle \right|^2 = |\tilde{U}_{\alpha\beta}(L)|^2 = \left| \sum_i U_{\alpha j}^* U_{\beta j} e^{-i\frac{m_j^2 L}{2E}} \right|^2. \quad (15)$$

Similarly, the survival probability  $P_S$  of the initial arbitrary flavor state  $|\nu_\alpha(0)\rangle$  can be obtained as

$$P_S = P_{\alpha \rightarrow \alpha} = |\langle \nu_\alpha(L) | \nu_\alpha \rangle|^2 = |\tilde{U}_{\alpha\alpha}(L)|^2. \quad (16)$$

## B. Oscillations in matter

When neutrinos enter the earth's atmosphere, the driving Hamiltonian can be represented as an effective Hamiltonian,

which is a sum of kinetic energy + potential energy [50]. For the three-flavor case, the effective Hamiltonian describing neutrino oscillations in matter is [65, 119]

$$\begin{aligned} \mathcal{H}_M &= \mathcal{H}_{vac} + \mathcal{H}_{int} = \mathcal{H}_{\mathcal{KE}} + \mathcal{H}_{\mathcal{PE}} \\ &= \frac{1}{2E} \left( U_{\text{PMNS}} \mathbb{M}^2 U_{\text{PMNS}}^\dagger + \mathbb{A} \right), \end{aligned} \quad (17)$$

where

$$\mathbb{A} = \begin{pmatrix} A_{CC} & 0 & 0 \\ 0 & 0 & 0 \\ 0 & 0 & 0 \end{pmatrix}, \quad A_{CC} \equiv 2EV_{CC} = 2\sqrt{2}EG_F N_e. \quad (18)$$

The kinetic energy part stems from the neutrino oscillation in vacuum, and the potential part originates from neutrino's interaction with matter, known as the Wolfenstein potential ( $A_{CC}$ ), relevant for neutrino oscillations in the earth-matter background [67, 120]. Neutrinos interact with matter due to coherent forward elastic scattering (and for negligible non-coherent effects) with the matter's electrons, generating charged-current (CC) potential ( $V_{CC}$ ). Here, the  $G_F = 1.6637 \times 10^{-5} \text{ GeV}^{-2}$  is the Fermi constant and  $N_e$  is the electron number density. In order to preserve a structure similar to that of the vacuum (see eqn. (11)), the effective Hamiltonian, eqn. (17), can be diagonalized via an orthogonal transformation as [65, 66, 108]

$$\mathcal{H}_M = \frac{1}{2E} \left( (U_{\text{PMNS}})_M (\mathbb{M}^2)_M (U_{\text{PMNS}})_M^\dagger \right), \quad (19)$$

where  $(U_{\text{PMNS}})_M (U_{\text{PMNS}})_M^\dagger = I$  and  $(U_{\text{PMNS}})_M \equiv U_{\text{PMNS}}((\theta_{ij})_M, \delta_{CP})$ , with the suffix M denoting parameters related to the matter case, i.e.,  $(\theta_{12})_M$  and  $(\theta_{13})_M$ . The neutrino squared-mass differences ( $\Delta m_{21}^2$  and  $\Delta m_{31}^2$ ) in vacuum can be related to the squared-mass differences in matter ( $(\Delta m_{21}^2)_M$  and  $(\Delta m_{31}^2)_M$ ) as

$$\begin{aligned} (\Delta m_{21}^2)_M &= \Delta m_{21}^2 \sqrt{\left( \cos 2\theta_{12} - \frac{a_{12}}{\Delta m_{21}^2} \right)^2} \\ &\quad + \cos^2(\theta_{13} - (\theta_{13})_M) \sin^2 2\theta_{12}, \end{aligned} \quad (20)$$

and

$$\begin{aligned} (\Delta m_{31}^2)_M &= \Delta m_{31}^2 + \frac{1}{4} A_{CC} \\ &\quad + \frac{1}{2} \left( (\Delta m_{21}^2)_M - \Delta m_{21}^2 \right) + \frac{3}{4} \left( (\Delta m_{ee}^2)_M - \Delta m_{ee}^2 \right), \end{aligned} \quad (21)$$

respectively. Here,  $a_{12} = \frac{1}{2}(A_{CC} + \Delta m_{ee}^2 - (\Delta m_{ee}^2)_M)$ , where  $\Delta m_{ee}^2 = c_{12}^2 \Delta m_{31}^2 + s_{12}^2 \Delta m_{32}^2$  is the effective squared-mass difference in vacuum, and its corresponding quantity in matter is  $(\Delta m_{ee}^2)_M = \Delta m_{ee}^2 \sqrt{\left( \cos 2\theta_{13} - \frac{A_{CC}}{\Delta m_{ee}^2} \right)^2 + \sin^2 2\theta_{13}}$  [121]. Furthermore, the neutrino vacuum mixing angle parameters  $\theta_{ij}$  can be related to matter mixing angle parameters  $((\theta_{ij})_M)$  as [65]

$$\sin(\theta_{12})_M = \sqrt{\frac{1}{2} - (\Delta m_{21}^2 \cos 2\theta_{12} - a_{12}) / (2(\Delta m_{ee}^2)_M)}, \quad (22)$$

$$\sin(\theta_{13})_M = \sqrt{\frac{1}{2} - (\Delta m_{ee}^2 \cos 2\theta_{13} - A_{CC})/2(\Delta m_{ee}^2)_M}, \quad (23)$$

$$(\theta_{23})_M = \theta_{23}. \quad (24)$$

Thus, the effective Hamiltonian in matter assumes a diagonal form.

#### IV. QUANTUM SPEED LIMIT TIME OF TWO-FLAVOR NEUTRINO OSCILLATIONS

In this section, building upon the description provided in section II, we first explore the quantum speed limit (QSL) time for the evolution of two-flavor neutrino states in the presence of matter backgrounds. Later, we investigate the QSL time for entanglement entropy in the two-flavor neutrino oscillations in matter.

##### A. QSL time for evolution of two-flavor neutrino states in matter

In the two-flavor neutrino oscillations in vacuum, at time  $t=0$ , the neutrino flavor state can be written as [41]

$$\begin{pmatrix} |\nu_\alpha\rangle \\ |\nu_\beta\rangle \end{pmatrix} = U(\theta) \begin{pmatrix} |\nu_j\rangle \\ |\nu_k\rangle \end{pmatrix}, \quad (25)$$

where  $\alpha, \beta = e, \mu, \tau$ ;  $j, k = 1, 2, 3$  and  $UU^\dagger = I$ ,

$$U(\theta) = \begin{pmatrix} U_{e1}^* & U_{e2}^* \\ U_{\mu 1}^* & U_{\mu 2}^* \end{pmatrix} \equiv \begin{pmatrix} \cos \theta & \sin \theta \\ -\sin \theta & \cos \theta \end{pmatrix}. \quad (26)$$

When the neutrino starts propagating in matter, its vacuum Hamiltonian  $\mathcal{H}_{vac}$ , eqn. (11), changes into the effective Hamiltonian in two-flavor scenario as [41, 67, 120]

$$\mathcal{H}_M = \frac{1}{4E} \left[ \begin{pmatrix} -\Delta m^2 \cos 2\theta & \Delta m^2 \sin 2\theta \\ \Delta m^2 \sin 2\theta & \Delta m^2 \cos 2\theta \end{pmatrix} + \begin{pmatrix} A_{CC} & 0 \\ 0 & -A_{CC} \end{pmatrix} \right], \quad (27)$$

where  $\Delta m^2 \equiv m_2^2 - m_1^2$  and  $\theta$  are the squared-mass difference and mixing angle in vacuum, respectively. The evolution equation for two flavour neutrino in matter is

$$i \frac{d}{dt} |\nu_\alpha\rangle = H_M |\nu_\alpha\rangle. \quad (28)$$

The effective Hamiltonian  $\mathcal{H}_M$  in matter is Hermitian  $\mathcal{H}_M^\dagger = \mathcal{H}_M$  and can be diagonalized by the orthogonal transformation

$$\mathcal{H}_M = \frac{1}{4E} (U_M (\mathbb{M}_M)^2 U_M^\dagger), \quad (29)$$

where  $(\mathbb{M}_M)^2 = \frac{1}{4E} \text{diag}(-\Delta m_M^2, \Delta m_M^2)$ . The unitary matrix

$$U_M(\theta_M) = \begin{pmatrix} \cos \theta_M & \sin \theta_M \\ -\sin \theta_M & \cos \theta_M \end{pmatrix}, \quad (30)$$

$\Delta m^2$	$\theta$	Energy
$7.41 \times 10^{-5} \text{ eV}^2$	$33.41^\circ$	1 GeV

TABLE I: The list of neutrino mixing parameters [122, 123].

is the effective mixing matrix in matter. The neutrino squared-mass difference and mixing angle in vacuum are related to matter parameters as [41]

$$\Delta m_M^2 = \sqrt{(\Delta m^2 \cos 2\theta - A_{CC})^2 + (\Delta m^2 \sin 2\theta)^2}, \quad (31)$$

and

$$\tan 2\theta_M = \frac{\tan 2\theta}{1 - \frac{A_{CC}}{\Delta m^2 \cos 2\theta}}. \quad (32)$$

respectively. Using eqn. (30) in eqn. (29), and using eqn. (28), the time-evolved neutrino flavor state  $|\nu_\alpha(t)\rangle$  in the presence of matter background can be written as

$$\begin{aligned} |\nu_\alpha(t)\rangle &= e^{-i\mathcal{H}_M t} |\nu_\alpha(0)\rangle \\ &= U_M \Lambda_M(t) U_M^\dagger |\nu_\alpha(0)\rangle \\ &= U_M \begin{pmatrix} e^{i\Delta m_M^2 \frac{t}{4E}} & 0 \\ 0 & e^{-i\Delta m_M^2 \frac{t}{4E}} \end{pmatrix} U_M^\dagger |\nu_\alpha(0)\rangle \\ &= \begin{pmatrix} \tilde{\mathcal{A}}_{\alpha\alpha}(t) & \tilde{\mathcal{A}}_{\alpha\beta}(t) \\ \tilde{\mathcal{A}}_{\beta\alpha}(t) & \tilde{\mathcal{A}}_{\beta\beta}(t) \end{pmatrix} |\nu_\alpha(0)\rangle. \end{aligned} \quad (33)$$

Thus, from eqn. (33), the time-evolved flavor neutrino state  $|\nu_\alpha(t)\rangle$  can be written in a coherent superposition of flavor basis in matter as

$$|\nu_\alpha(t)\rangle = \tilde{\mathcal{A}}_{\alpha\alpha}(t) |\nu_\alpha\rangle + \tilde{\mathcal{A}}_{\alpha\beta}(t) |\nu_\beta\rangle, \quad (34)$$

where  $|\tilde{\mathcal{A}}_{\alpha\alpha}(t)|^2 + |\tilde{\mathcal{A}}_{\alpha\beta}(t)|^2 = 1$ . In the ultra-relativistic approximation ( $t \approx L$ ), the survival probability of the time-evolved flavor neutrino states  $|\nu_\alpha(t)\rangle$  in the earth-matter background (when  $A_{CC} \neq 0$ ) is given as  $P_S^{\text{Matter}} = |\langle \nu_\alpha(L) | \nu_\alpha \rangle|^2 = |\tilde{\mathcal{A}}_{\alpha\alpha}(L)|^2$ . For any initial neutrino state in matter

$$P_S^{\text{Matter}} = 1 - \sin^2(2\theta_M) \sin^2(\phi_M), \quad (35)$$

where  $\phi_M = \frac{\Delta m_M^2 L}{4E}$ . We use the electron matter density near the earth,  $N_e \approx 2.8 \text{ gm/cm}^3$ , and neutrino energy,  $E \approx \mathcal{O}(\text{GeV})$ . The potential of coherent forward elastic scattering with matter electrons  $A_{CC}$  corresponds to  $A_{CC} \approx \mathcal{O}(10^{-4}) \text{ eV}^2$ .

Since  $\theta_M$  and  $\Delta m_M^2$  are dependent on  $A_{CC}$ ,  $P_S^{\text{Matter}}$  (eqn. (35)) may be analysed as a function of a constant earth-matter potential  $A_{CC}$ . When  $A_{CC} = 0$ , the survival probability of the initial state  $|\nu_\alpha\rangle$  in matter, eqn. (35), reduces to its vacuum counterpart  $P_S^{\text{vacuum}} = |\langle \nu_\alpha(L) | \nu_\alpha \rangle|^2$  which is

$$P_S^{\text{vacuum}} = 1 - \sin^2(2\theta) \sin^2(\phi), \quad (36)$$

where  $\phi = \frac{\Delta m^2 L}{4E}$ . In the analysis of neutrino oscillation experimental data, the oscillatory term in eqn. (36),  $\sin^2(\phi)$ , can be simplified to the following convenient form:  $\sin^2(\frac{\Delta m^2 L}{4E}) \equiv$

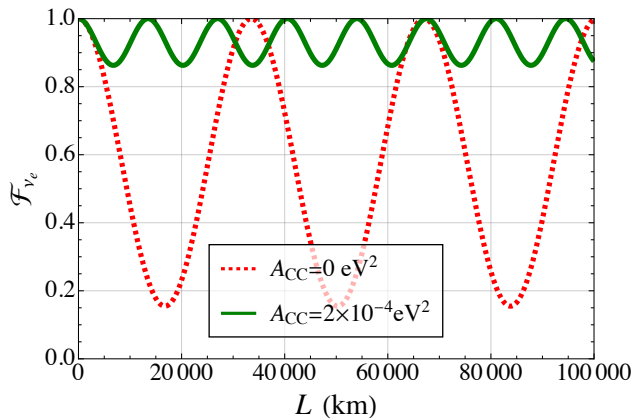


FIG. 1: In the two-flavor neutrino oscillation, the fidelity  $\mathcal{F}_{\nu_e}$  of the initial electron neutrino state  $|\nu_e\rangle$  is depicted as a function of propagation length  $L$  (km). This representation includes vacuum ( $A_{CC} = 0$ ), indicated by a red dashed line and a constant matter potential ( $A_{CC} = 2 \times 10^{-4} \text{eV}^2$ ), represented by a green solid line. The various neutrino mixing parameters used are taken from Table I.

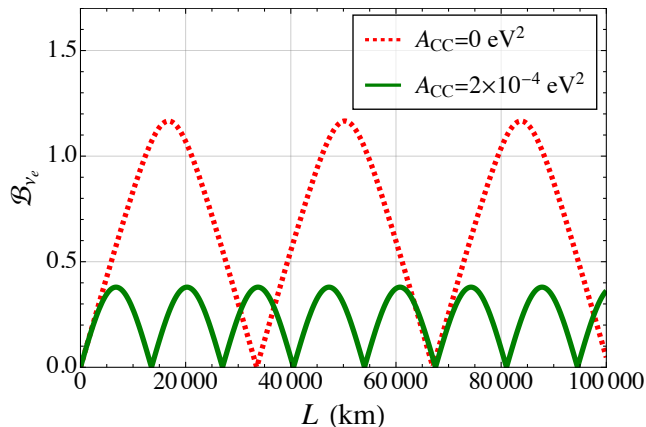


FIG. 2: In the two-flavor neutrino oscillation, the Bures angle  $\mathcal{B}_{\nu_e}$  of the initial electron neutrino state  $|\nu_e\rangle$  is plotted as a function of propagation length  $L$  (km). This representation includes vacuum ( $A_{CC} = 0$ ) indicated by a red dashed line and in a constant matter potential ( $A_{CC} = 2 \times 10^{-4} \text{eV}^2$ ) represented by a green solid line. The various neutrino mixing parameters used are taken from Table I.

$\sin^2\left(\frac{\Delta m^2 L c^3}{4\hbar E}\right) \rightarrow \sin^2(1.27\Delta m^2(\text{eV}^2)\frac{L(\text{km})}{E(\text{GeV})})$ . The list of neutrino mixing parameters used for our analysis is detailed in Table I.

In general, comparing two quantum states and assessing their closeness is pertinent, especially in experimental settings where the observed quantum state needs to be compared with theoretical predictions. A valuable measure for this comparison is fidelity, denoted by  $\mathcal{F}$ . In the context of two-flavor neu-

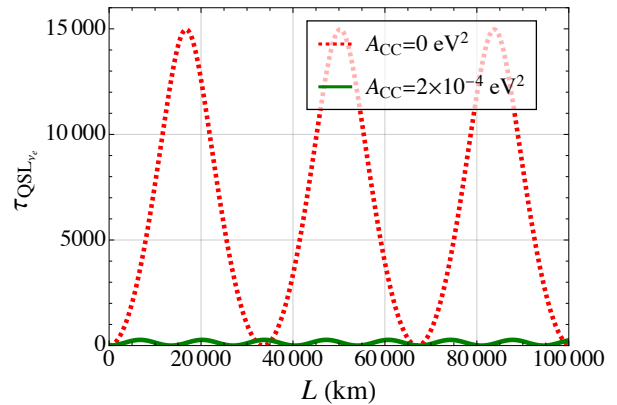


FIG. 3: In the two-flavor neutrino oscillation, the QSL time  $\tau_{\text{QSL}_{\nu_e}}$  is depicted for the initial electron neutrino state  $|\nu_e\rangle$  as a function of propagation length  $L$  (km). This is represented in vacuum ( $A_{CC} = 0$ ) by a red dashed line and in a constant matter potential ( $A_{CC} = 2 \times 10^{-4} \text{eV}^2$ ) by a green solid line. The various neutrino mixing parameters used are taken from Table I.

trino oscillations, undergoing unitary evolution, the fidelity can be equated to the survival probability of the initial flavor neutrino states  $|\nu_\alpha\rangle$  in the matter background as

$$\mathcal{F}_{\nu_\alpha}(|\nu_\alpha(0)\rangle, |\nu_\alpha(t)\rangle) = P_S^{\text{Matter}}. \quad (37)$$

We assume the initial state to be an electron neutrino, i.e.,  $\alpha = e$ . Fig. 1 illustrates the fidelity  $\mathcal{F}_{\nu_e}$  of the initial electron flavor neutrino state  $|\nu_e\rangle$  as a function of propagation length  $L$  (km) in vacuum and in a constant earth-matter background. Here, the red dashed line and green solid line represent  $\mathcal{F}_{\nu_e}$  for the state  $|\nu_e(t)\rangle$  in vacuum ( $A_{CC} = 0$ ), in a constant earth-matter potential ( $A_{CC} = 2 \times 10^{-4} \text{eV}^2$ ), respectively. We observe that at  $L = 0$ ,  $\mathcal{F}_{\nu_e} = 1$ . As  $L$  increases,  $\mathcal{F}_{\nu_e}$  varies periodically for the two different matter backgrounds. Using eqn. (37) in eqn. (2), the Bures angle of the state  $|\nu_e(t)\rangle$  can be calculated as

$$\mathcal{B}_{\nu_e} = \cos^{-1} \sqrt{\mathcal{F}_{\nu_e}(|\nu_e(0)\rangle, |\nu_e(t)\rangle)}. \quad (38)$$

In Fig. 2, the Bures angle  $\mathcal{B}_{\nu_e}$  is plotted as a function of propagation length  $L$  (in kilometers) for the initial state  $|\nu_e\rangle$  in vacuum (red dashed line) and in the presence of a constant earth-matter potential (green solid line). This graph illustrates the proximity between the initial and final states. We observe that the periodic behavior of  $\mathcal{B}_{\nu_e}$  persists as the propagation length increases.

Furthermore, we utilize eqns. (29) and (34) in eqn. (4) to calculate the time-averaged mean energy. Subsequently, employing these time-averaged mean values, and the Bures angle, eqn. (38), in eqn. (3), we numerically compute the quantum speed limit time,  $\tau_{\text{QSL}}$ , for the initial electron neutrino flavor state  $|\nu_e\rangle$  in vacuum and in a constant earth-matter background. The effect of matter on  $\tau_{\text{QSL}_{\nu_e}}$ , as a function of propagation length  $L$  (km), is illustrated in Fig. 3. It is observed that

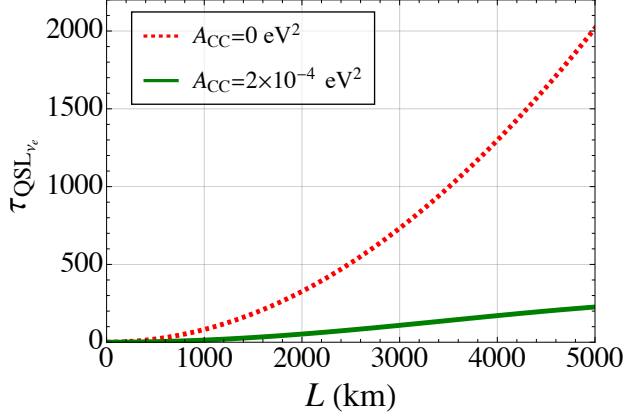


FIG. 4: In the two-flavor neutrino oscillation, we depict the QSL time  $\tau_{\text{QSL}_{\nu_e}}$  for the initial electron neutrino state  $|\nu_e\rangle$  as a function of propagation length  $L$  (km) upto a length of  $L \approx 5000$  (km). This is shown in vacuum ( $A_{\text{CC}} = 0$ ) with a red dashed line and in a constant matter potential ( $A_{\text{CC}} = 2 \times 10^{-4} \text{ eV}^2$ ) with a green line. The various neutrino mixing parameters used are taken from Table I.

$\tau_{\text{QSL}_{\nu_e}}$  exhibits periodicity in vacuum (red dashed line) and in the constant earth-matter potential (green solid line) as the propagation length increases. It is worth mentioning here that when  $\tau_{\text{QSL}}/L$  equals 1, the dynamic evolution of the neutrino state remains unchanged. In other words, the evolution speed has already reached its maximum. Conversely,  $\tau_{\text{QSL}}/L < 1$  indicates the potential for the dynamic evolution of the neutrino state to speed up. The smaller the value of  $\tau_{\text{QSL}}/L$ , the greater the potential for a quantum speedup. From Fig. 3, we observe that for the state  $|\nu_e(t)\rangle$ , the ratio of  $\tau_{\text{QSL}_{\nu_e}}/L < 1$ , lesser for evolution in matter as compared to that in vacuum. Thus, a rapid evolution of the neutrino state is observed in matter (green solid line) compared to vacuum (red dashed line). This result is further illustrated in Fig. 4, where we zoom into Fig. 3 up to a propagation length of  $L \approx 5000$  (km).

### B. QSL time for entanglement in two-flavor neutrino oscillations in matter

In this subsection, we initially employ the principles of quantum information theory to map neutrino flavor eigenstates at time  $t = 0$  onto a two-qubit-mode state as follows [69–88]:

$$|\nu_\alpha\rangle \equiv |1\rangle_\alpha \otimes |0\rangle_\beta \equiv |10\rangle; \quad |\nu_\beta\rangle \equiv |0\rangle_\alpha \otimes |1\rangle_\beta \equiv |01\rangle. \quad (39)$$

Under the ultra-relativistic approximation, neutrino flavor eigenstates can be considered as distinct modes. Entanglement represents a connection between the quantum states of the two modes. A specific form of entanglement that arises among various modes is termed “neutrino mode (flavor) entanglement”. Consequently, the time-evolved flavor state can

be understood as an entangled superposition of flavor modes. This concept can be investigated within the framework of both two- and three-flavor neutrino oscillations. In the context of two-flavor neutrino oscillations, using eqn. (39) in eqn. (34), the time-evolved flavor neutrino state in the presence of a constant earth-matter background can be represented as a two-qubit system

$$|\nu_\alpha(t)\rangle = \tilde{\mathcal{A}}_{\alpha\alpha}(t) |10\rangle + \tilde{\mathcal{A}}_{\alpha\beta}(t) |01\rangle. \quad (40)$$

The corresponding density matrix of the state  $|\nu_\alpha(t)\rangle$  in the presence of a constant earth-matter background is

$$\rho(t) = |\nu_\alpha(t)\rangle \langle \nu_\alpha(t)| = \begin{pmatrix} 0 & 0 & 0 & 0 \\ 0 & |\tilde{\mathcal{A}}_{\alpha\alpha}(t)|^2 & \tilde{\mathcal{A}}_{\alpha\alpha}(t)\tilde{\mathcal{A}}_{\alpha\beta}^*(t) & 0 \\ 0 & \tilde{\mathcal{A}}_{\alpha\beta}(t)\tilde{\mathcal{A}}_{\alpha\alpha}^*(t) & |\tilde{\mathcal{A}}_{\alpha\beta}(t)|^2 & 0 \\ 0 & 0 & 0 & 0 \end{pmatrix}, \quad (41)$$

where  $\rho(t) = \rho^2(t)$  is an idempotent matrix and  $\text{Tr}(\rho^2(t)) = 1$ . This implies that the state  $\rho(t)$  is a pure-state. However, the reduced state (by tracing over the other qubit)  $\rho_\alpha(t) = \text{Tr}_\beta(\rho(t))$  and  $\rho_\beta(t) = \text{Tr}_\alpha(\rho(t))$  follows  $\text{Tr}(\rho_\alpha^2(t)) < 1$  and  $\text{Tr}(\rho_\beta^2(t)) < 1$ , which are in the mixed states. This shows that the state  $|\nu_\alpha(t)\rangle$  is a bi-partite quantum system of a two-qubit pure state. This is also true for the state  $|\nu_\beta(t)\rangle$ . The eigenvalues of the reduced state are  $\rho_\alpha(t)$  are  $\lambda_1, \lambda_2$ . These two eigenvalues are the survival ( $\lambda_1 = P_S = |\tilde{\mathcal{A}}_{\alpha\alpha}(t)|^2$ ) and the oscillation ( $\lambda_2 = P_O = |\tilde{\mathcal{A}}_{\alpha\beta}(t)|^2 = 1 - P_S$ ) probabilities of the initial state  $|\nu_\alpha\rangle$  in matter background. Using eqn. (5) and the eigenvalues of the reduced state  $\rho_\alpha(t)$ , the bipartite entanglement entropy  $S_{EE}(t)$  of the reduced state  $\rho_\alpha(t)$  can be calculated as

$$S_{EE}(\rho_\alpha(t)) = -|\tilde{\mathcal{A}}_{\alpha\alpha}(t)|^2 \log_2 |\tilde{\mathcal{A}}_{\alpha\alpha}(t)|^2 - (1 - |\tilde{\mathcal{A}}_{\alpha\alpha}(t)|^2) \log_2 (1 - |\tilde{\mathcal{A}}_{\alpha\alpha}(t)|^2). \quad (42)$$

Consequently, using eqn. (7), the capacity of entanglement  $C_E$  of the reduced state  $\rho_\alpha(t)$  is obtained as

$$C_E(\rho_\alpha(t)) = |\tilde{\mathcal{A}}_{\alpha\alpha}(t)|^2 \log_2^2 |\tilde{\mathcal{A}}_{\alpha\alpha}(t)|^2 + (1 - |\tilde{\mathcal{A}}_{\alpha\alpha}(t)|^2) \log_2^2 (1 - |\tilde{\mathcal{A}}_{\alpha\alpha}(t)|^2) - (|\tilde{\mathcal{A}}_{\alpha\alpha}(t)|^2 \log_2 |\tilde{\mathcal{A}}_{\alpha\alpha}(t)|^2 - (1 - |\tilde{\mathcal{A}}_{\alpha\alpha}(t)|^2) \log_2 (1 - |\tilde{\mathcal{A}}_{\alpha\alpha}(t)|^2))^2. \quad (43)$$

The bipartite entanglement measures quantified in eqns. (42) and (43) are directly associated with two measurable quantities, survival ( $P_S$ ) and oscillation ( $P_O$ ) probabilities, enabling straightforward connections with experimentally determined values of neutrino mixing parameters. One of the prominent bipartite entanglement measures, concurrence, can be related to  $P_S$  and  $P_O$  of two-flavor neutrino oscillations as  $C(\rho_\alpha(t)) = 2\sqrt{P_S P_O}$  [74]. This implies  $P_S = 1 - \frac{1}{2}\sqrt{1 - C^2(\rho_\alpha(t))}$  and  $P_O = \frac{1}{2}\sqrt{1 - C^2(\rho_\alpha(t))}$ . Hence, the entanglement entropy  $S_{EE}(\rho_\alpha(t))$ , eqn. (42), can

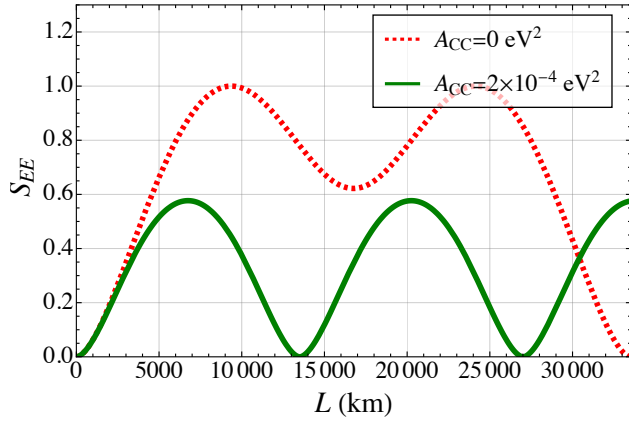


FIG. 5: In the two-flavor neutrino oscillation, the entanglement entropy ( $S_{EE}(\rho_e(t))$ ), for the initial state  $|v_e\rangle$ , is shown as a function of propagation length  $L$  (km). This is represented in vacuum ( $A_{CC} = 0$ ) by a red dashed line and in a constant matter potential ( $A_{CC} = 2 \times 10^{-4} \text{eV}^2$ ) by a green solid line. The various neutrino mixing parameters used are taken from Table I.

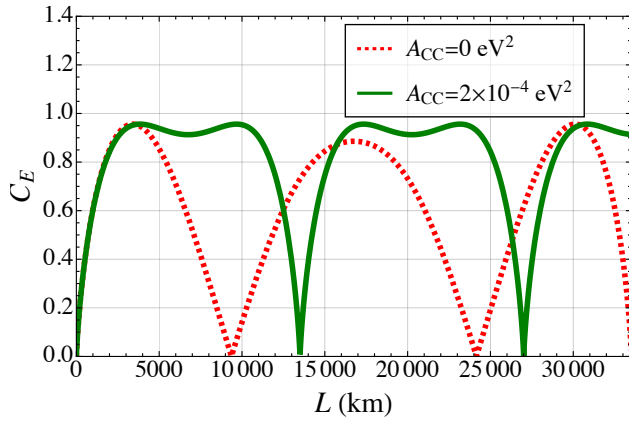


FIG. 6: In the two-flavor neutrino oscillation, the capacity of entanglement ( $C_E(\rho_e(t))$ ), for the initial state  $|v_e\rangle$ , is depicted as a function of propagation length  $L$  (km). This is represented in vacuum ( $A_{CC} = 0$ ) by a red dashed line and in a constant matter potential ( $A_{CC} = 2 \times 10^{-4} \text{eV}^2$ ) by a green solid line. The various neutrino mixing parameters used are taken from Table I.

be re-expressed in terms of concurrence as

$$S_{EE}(C(\rho_\alpha(t))) = \left(1 - \frac{1}{2} \sqrt{1 - C^2(\rho_\alpha(t))}\right) \log_2 \left(1 - \frac{1}{2} \sqrt{1 - C^2(\rho_\alpha(t))}\right) - \frac{1}{2} \sqrt{1 - C^2(\rho_\alpha(t))} \log_2 \left(\frac{1}{2} \sqrt{1 - C^2(\rho_\alpha(t))}\right). \quad (44)$$

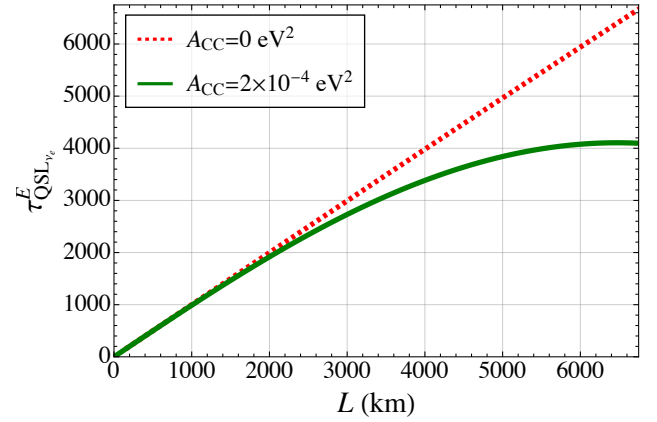


FIG. 7: QSL time for entanglement entropy  $\tau_{QSL_{v_e}}^E$ , for the initial state  $|v_e\rangle$ , as a function of propagation length  $L$  (km) for two-flavor neutrino oscillations. This is represented in vacuum ( $A_{CC} = 0$ ) by a red dashed line and in a constant matter potential ( $A_{CC} = 2 \times 10^{-4} \text{eV}^2$ ) by a green solid line. The various neutrino mixing parameters used are taken from Table I.

Since,  $P_S > 0$  implies  $P_O < 1$ , which in term implies  $C(\rho_\alpha(t)) \neq 0$ . Consequently,  $S_{EE}(C(\rho_\alpha(t))) \neq 0$ . Similarly, one can also relate capacity of entanglement, eqn. (43), as a function of concurrence. In this vein, various other bipartite entanglement measures, such as Bell's inequality violation, teleportation fidelity, geometric discord, tangle, linear entropy, negativity, among others, have previously been investigated and simplified in terms of two-flavor neutrino survival and oscillation probabilities [69, 74, 79].

In Figs. 5 and 6, in the ultra-relativistic approximation ( $t \approx L$ ), the entanglement entropy  $S_{EE}(\rho_e(t))$  and the capacity of entanglement  $C_E(\rho_e(t))$ , respectively, are plotted as a function of propagation length ( $L$  in kilometers) for the initial electron flavor neutrino state  $|v_e\rangle$ , particularly in vacuum (red dashed line) and in the presence of a constant earth-matter potential (green solid line). We observe that at  $L = 0$ , the entanglement entropy ( $S_{EE}(\rho_e(t))$ ) is zero, indicating that  $|v_e(t)\rangle$  is in a separable state. Moreover, as  $L$  increases ( $L > 0$ ),  $S_{EE}(\rho_e(t))$  develops periodically and monotonically towards its maximum across vacuum and matter backgrounds. Additionally, we observe a separation in entanglement entropy in the presence of matter compared to vacuum. In Fig. 6, the capacity of entanglement  $C_E$  (or the variance in the entanglement entropy) approaches zero when neutrino oscillates in vacuum (red dashed line), in both the maximally entangled and separable state limits. However,  $C_E$  attains a maximum in a partially entangled state. Additionally, for neutrino oscillations in matter (green solid line),  $C_E$  reaches its maximum value for a partially entangled state, but there is a dip in  $C_E$  when the  $S_{EE}$  is maximum. The entanglement entropy (or capacity of entanglement) attains its maximum (or minimum) when the survival and oscillation probabilities are equal, i.e.,  $|\tilde{\mathcal{A}}_{ee}(t)|^2 = 1 - |\tilde{\mathcal{A}}_{ee}(t)|^2 = \frac{1}{2}$ . Hence, in the two-qubit system, at  $L > 0$ ,  $S_{EE}(\rho_e(t)) \neq 0$  and  $C_E(\rho_e(t)) \neq 0$  identify

that the time-evolved electron flavor neutrino state  $|v_e(t)\rangle$  is a bipartite two-qubit pure entangled state. The  $|v_e(t)\rangle$  produces flavor eigenstates of  $|v_\alpha\rangle$  and  $|v_\beta\rangle$ , similar to the Bell's state/two-qubit state used in quantum information. Moreover, in Fig. (7), using eqns. (42) and (43) in eqn. (6), the QSL time for the entanglement entropy  $\tau_{\text{QSL}}^E$  of  $|v_e(t)\rangle$  is estimated as a function of propagation length ( $L$  in kilometers) across vacuum (red dashed line) and in a constant earth-matter potential backgrounds (green solid line). Under the QSL time-bound condition  $\tau_{\text{QSL}}^E/L < 1$ , we observe a quick suppression of entanglement in matter compared to vacuum as the propagation length increases.

## V. QUANTUM SPEED LIMIT TIME FOR EVOLUTION OF THE THREE-FLAVOR NEUTRINO STATE IN MATTER

In the three-flavor neutrino oscillations, using the effective Hamiltonian, eqn. (19), the time-evolved neutrino states in vacuum, eqn. (14), starting from the muon flavor, gets modified in the presence of matter as [50, 79]

$$|v_\mu(t)\rangle = \tilde{\mathcal{A}}_{\mu e}(t)|v_e\rangle + \tilde{\mathcal{A}}_{\mu\mu}(t)|v_\mu\rangle + \tilde{\mathcal{A}}_{\mu\tau}(t)|v_\tau\rangle, \quad (45)$$

where  $|\tilde{\mathcal{A}}_{\mu\mu}(t)|^2 + |\tilde{\mathcal{A}}_{\mu e}(t)|^2 + |\tilde{\mathcal{A}}_{\mu\tau}(t)|^2 = 1$ . As a result, the survival and oscillation probabilities of the three-flavor state  $|v_\mu(t)\rangle$  in matter are determined as  $P_{\mu\rightarrow\mu} = |\tilde{\mathcal{A}}_{\mu\mu}(t)|^2$ ,  $P_{\mu\rightarrow e} = |\tilde{\mathcal{A}}_{\mu e}(t)|^2$ , and  $P_{\mu\rightarrow\tau} = |\tilde{\mathcal{A}}_{\mu\tau}(t)|^2$ , respectively. The issue of neutrino mass hierarchy is closely linked to current experimental data on neutrino survival and oscillation probabilities, permitting two potential classes of solutions [50]. In the Normal Hierarchy (NH) scenario, the two lightest mass eigenstates demonstrate a marginal mass difference, while the third eigenstate is heavier such that  $m_3 > m_2 > m_1$ . Conversely, in the Inverted Hierarchy (IH), the lightest mass eigenstate precedes a doublet of higher mass eigenstates. Within this doublet, there again exists a mass difference. Hence,  $m_3 < m_2 < m_1$ . The neutrino mixing parameters  $\Delta m_{lk}^2$ ,  $\theta_{ij}$ , and  $\delta_{\text{CP}}$ , along with their  $1\sigma$  best-fit data for normal and inverted hierarchy, are presented in Tables II and III, respectively. Note that here  $\Delta m_{3l}^2 = \Delta m_{31}^2 > 0$  for NH and  $\Delta m_{3l}^2 = \Delta m_{32}^2 < 0$  for IH [122, 123].

Moreover, including various mass-squared differences and mixing angles as outlined in Tables II and III for the NH and IH scenarios. The survival and oscillation probabilities of the state  $|v_\mu(t)\rangle$  also rely on the ratio  $L/E$  (km/GeV), which can be fixed in various Long-Baseline accelerator neutrino source experiments setups like T2K, Nova, and DUNE, presenting a more realistic scenario for neutrino oscillations.

T2K (Tokai-to-Kamioka) [124] operates as an off-axis experiment employing a  $\nu_\mu$  neutrino beam originating at J-PARC (Japan Proton Accelerator Complex) with an energy range approximately between 100 MeV to 1 GeV and a baseline of 295 km.

NOvA (NuMI Off-Axis  $\nu_e$  Appearance) [125], a long baseline experiment, utilizes neutrinos from the NuMI (Neutrinos at the Main Injector) beamline at Fermilab optimized to observe  $\nu_\mu \rightarrow \nu_e$  oscillations. This experiment employs two detectors positioned 14 mrad off the axis of the NuMI beamline,

Parameters	Best fit $\pm 1\sigma$
$\theta_{12}/^\circ$	$33.41_{-0.72}^{+0.75}$
$\theta_{23}/^\circ$	$49.1_{-1.3}^{+1.0}$
$\theta_{13}/^\circ$	$8.54_{-0.12}^{+0.11}$
$\frac{\Delta m_{21}^2}{10^{-5}eV^2}$	$7.41_{-0.20}^{+0.21}$
$\frac{\Delta m_{3l}^2}{10^{-3}eV^2}$	$2.511_{-0.027}^{+0.028}$
$\delta_{\text{CP}}/^\circ$	$197_{-25}^{+42}$

TABLE II: In the three-flavor neutrino oscillation, the values of the neutrino mixing parameters for normal hierarchy (NH) that we considered in our analysis are taken from Ref. [122, 123] along with their corresponding  $1\sigma$  errors (90% CL).

Parameters	Best fit $\pm 1\sigma$
$\theta_{12}/^\circ$	$33.41_{-0.72}^{+0.75}$
$\theta_{23}/^\circ$	$49.5_{-1.2}^{+0.9}$
$\theta_{13}/^\circ$	$8.57_{-0.11}^{+0.12}$
$\frac{\Delta m_{21}^2}{10^{-5}eV^2}$	$7.41_{-0.20}^{+0.21}$
$\frac{\Delta m_{3l}^2}{10^{-3}eV^2}$	$-2.498_{-0.025}^{+0.032}$
$\delta_{\text{CP}}/^\circ$	$286_{-32}^{+27}$

TABLE III: In the three-flavor oscillation, the values of the neutrino mixing parameters for inverted hierarchy (IH) that we considered in our analysis are taken from Ref. [122, 123] along with their corresponding  $1\sigma$  errors (90% CL).

with the near and far detectors located at 1 km and 810 km from the source, respectively. The flavor composition of the beam consists of 92.9% of  $\nu_\mu$  and 5.8% of  $\bar{\nu}_\mu$  and 1.3% of  $\nu_e$  and  $\bar{\nu}_e$  with the energy of the neutrino beam varying from 1.5 GeV to 4 GeV.

Deep Underground Neutrino Experiment (DUNE) [62, 126, 127] is an experimental facility utilizing the NuMI neutrino beam with an energy range of 1 – 10 GeV from Fermilab and features a long baseline of 1300 km. This configuration enables an  $L/E$  ratio of about  $10^3$  km/GeV, providing good sensitivity for CP violation ( $\delta_{\text{CP}}$ ) measurement and determination of mass hierarchy.

The neutrino oscillation depends on a complex quantity in the PMNS mixing matrix related to a phase factor associated with CP violation,  $\delta_{\text{CP}}$  (as outlined in the PMNS matrix of eqn. (9)) [128–132]. However, the value of the CP-violating phase is still not well-constrained in neutrino experiments [53]. On the other hand, the  $\delta_{\text{CP}}$  is linked with matter-antimatter asymmetry (more baryons over anti-baryons) in the observable universe [133]. The hunt to find baryon number violation processes in nature has not been fruitful without caveats till now. However, if the number of leptons created in a reaction is not the same as the number destroyed, it could indirectly lead to a net change in the baryon number [134–146]. Neutrino, a lepton, can provide us with more insight into this. Comparing the difference between neutrino and anti-neutrino oscillations, ongoing long-baseline neutrino oscillation experiments, such as T2K and NOvA [50, 53, 124, 147–150] and

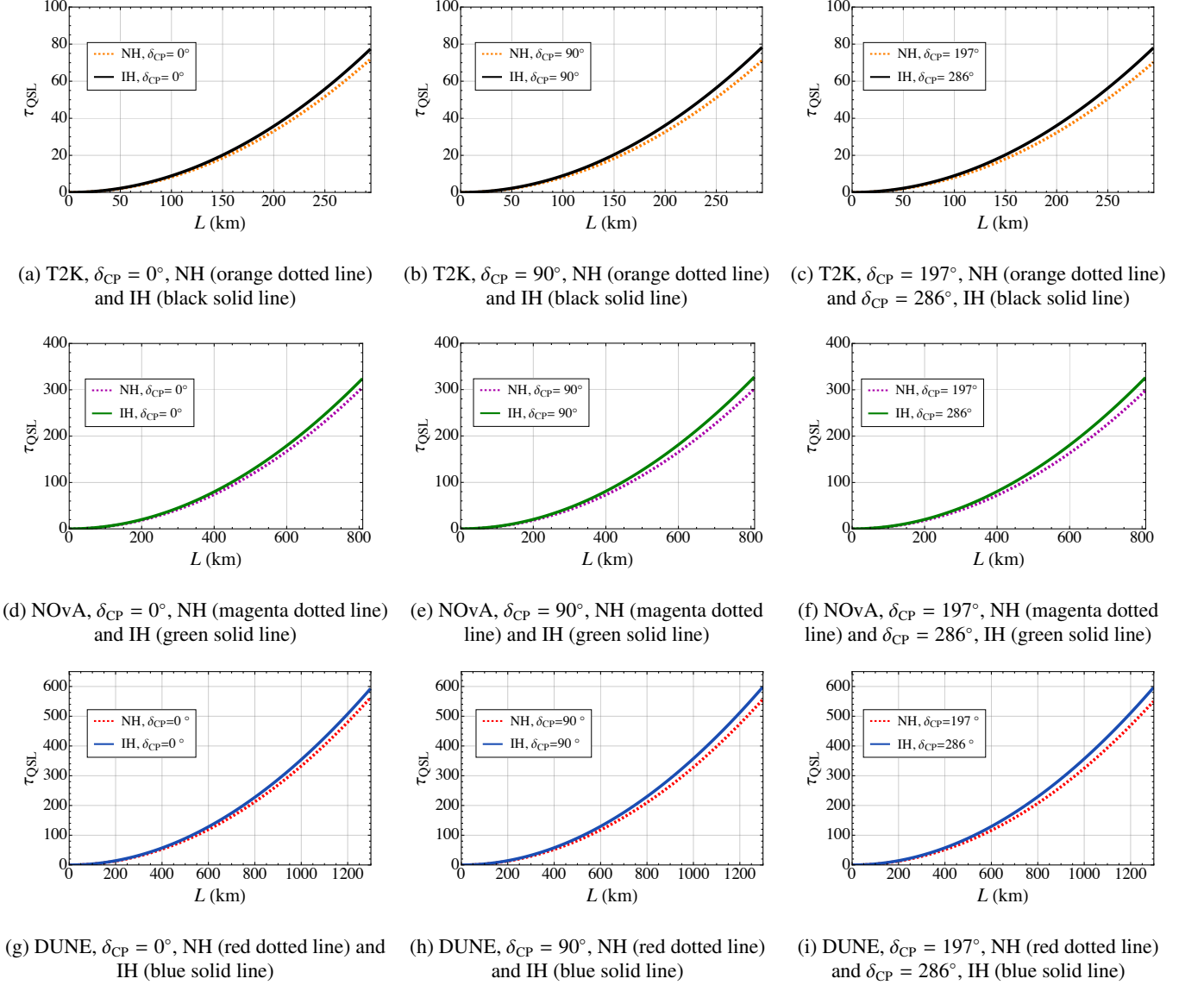


FIG. 8: In three-flavor neutrino oscillations, we compare the QSL time  $\tau_{QSL}$  versus  $L$  (km) for the initial muon flavor neutrino state  $|\nu_\mu\rangle$  in NH and IH. This comparison is illustrated using T2K, NOvA and DUNE data in Figs. (8a, 8b, 8c), Figs. (8d, 8e, 8f), and Figs. (8g, 8h, 8i), respectively, under distinct CP violation phases. The various neutrino mixing parameters used are taken from Tables II for NH and III for IH along with their corresponding  $1\sigma$  errors (90% CL).

also next-generation experiment, DUNE [126, 127, 151], has the potential to detect evidence for CP violation. The global fit values [122, 123] of  $\delta_{CP}$  in NH and IH are listed in Tables II and III, respectively.

The matter density in all these experiments is approximately 2.8gm/cc, corresponding to the constant density parameter  $A_{CC} \approx 1.01 \times 10^{-4} \text{eV}^2$ . Using eqn. (45) in eqn. (3), the QSL time ( $\tau_{QSL}$ ) of the state  $|\nu_\mu(t)\rangle$  in a constant earth-matter background, taking into account CP violation phases for both NH and IH scenarios can be studied. We explore these aspects across three Long-Baseline accelerator neutrino source data: T2K, NOvA, and DUNE.

In the ultra-relativistic approximation  $L \approx t$ , the top, mid-

dle, and bottom panels of Fig. 8 illustrate  $\tau_{QSL}$  versus  $L$ (km) of the time-evolved muon flavor neutrino state  $|\nu_\mu(t)\rangle$  in a constant earth-matter background at distinct CP violation phase values, under the assumptions of NH (Table II) and IH (Table III), and employing constraints on the ratio of  $L/E$  (km/GeV) provided in the long baseline experimental data such as T2K, NOvA and DUNE.

The top panel of Fig. 8 displays the minimum time required for the survival of the initial state  $|\nu_\mu\rangle$  in constant matter as a function of propagation length ( $L$ (km)) using the T2K length and energy scale. In Figs. (8a, 8b, 8c), near a length of 280 km, energy ( $\approx 1$  GeV), and considering distinct values of  $\delta_{CP}$  for the NH ( $\delta_{CP} = 0^\circ, 90^\circ, 197^\circ$ ) (orange dotted line) and for the

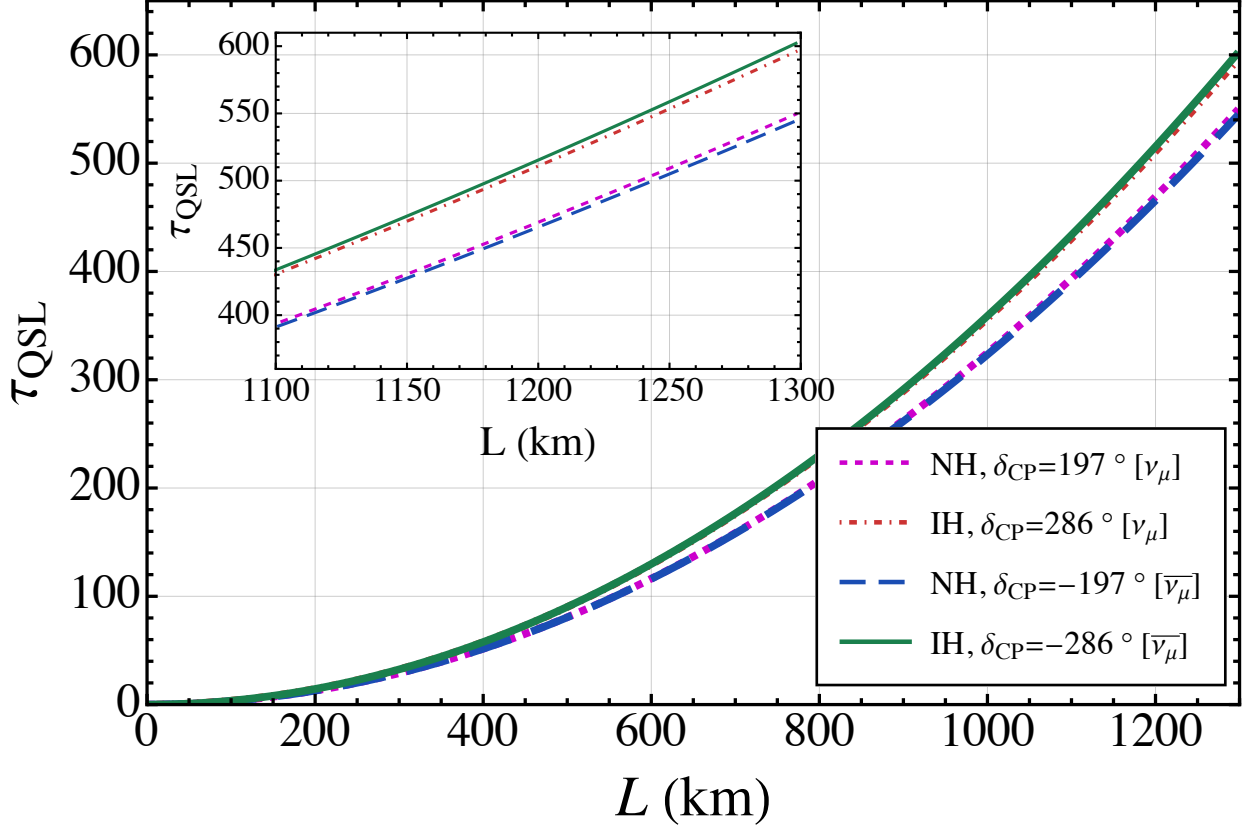


FIG. 9: In three-flavor neutrino oscillations, we compare the QSL time  $\tau_{\text{QSL}}$  versus  $L$  (km) for the initial muon flavor neutrino state  $|\nu_\mu\rangle$  (positive matter potential  $+A_{\text{CC}}$  and positive CP violating phase  $+\delta_{\text{CP}}$ ) and the initial anti-muon flavor neutrino state  $|\bar{\nu}_\mu\rangle$  (negative matter potential  $-A_{\text{CC}}$  and negative CP violating phase  $-\delta_{\text{CP}}$ ) in NH and IH. This comparison is illustrated in DUNE setup using global fit data [122, 123]. Also provided is a close-up view towards the end of the baseline in the top left corner.

IH ( $\delta_{\text{CP}} = 0^\circ, 90^\circ, 286^\circ$ ) (black solid line), we observe that the separation between  $\tau_{\text{QSL}}$  in NH (orange dotted line) and IH (black solid line) increases as the CP violation phase increases. Additionally, it is observed that under the time-bound condition  $\tau_{\text{QSL}}/L < 1$ , the initial state  $|\nu_\mu\rangle$  in the presence of a constant earth-matter potential in NH (orange dotted line) undergoes more speedup compared to the IH (black solid line) case.

Furthermore, within the middle panel of Fig. 8, we use the long baseline length scale ( $L \approx 800$ km) with energy  $E \approx 4$ GeV provided by NOvA data to examine the QSL time in NH and IH scenarios for the initial state  $|\nu_\mu\rangle$  propagating in a constant earth-matter background. We compare  $\tau_{\text{QSL}}$  versus  $L$  (km) of the state  $|\nu_\mu(t)\rangle$  in the NH (magenta dotted line) and IH (green solid line) scenarios in Figs. (8d, 8e, 8f). Notably, at larger CP violation phase values,  $\tau_{\text{QSL}}$  of the initial state  $|\nu_\mu\rangle$  in Fig. (8f) demonstrates a more pronounced separation between NH (magenta dotted line) and IH (green solid line) cases. According to the time-bound condition  $\tau_{\text{QSL}}/L < 1$ , the dynamic evolution of the initial state  $|\nu_\mu\rangle$  in matter demonstrates faster evolution for the case of NH (magenta dotted

line) as compared to the IH (green solid line), especially noticeable at substantial CP violation phases, as can be seen in Fig. 8f.

The bottom panel of Fig. 8 depicts  $\tau_{\text{QSL}}$  of the time-evolved muon flavor neutrino state  $|\nu_\mu(t)\rangle$  using the DUNE's baseline length ( $L \approx 1300$  km) and energy ( $\approx 3.5$  GeV). In Figs. (8g, 8h, 8i), we compute and compare  $\tau_{\text{QSL}}$  for the initial state  $|\nu_\mu\rangle$  as a function of propagation length  $L$  (km) for NH (red dotted line) and IH (blue solid line), and for distinct CP violation phase values. In all these figures, the results can distinguish between  $\tau_{\text{QSL}}$  for NH and IH. Fig. 8i highlights that under the constraint  $\tau_{\text{QSL}}/L < 1$ , the initial state  $|\nu_\mu\rangle$  undergoes fast evolution at a large CP violation phase in DUNE, particularly in the NH scenario. Hence, by using experimental data from T2K, NOvA, and DUNE, we observe that the faster evolution of neutrino muon flavor states in matter is sensitive to the significant CP violation phase in the NH scenario.

So far, we have considered  $\tau_{\text{QSL}}$  for the initial muon flavor neutrino state  $|\nu_\mu\rangle$ . For completeness, we discuss  $\tau_{\text{QSL}}$  for the initial muon anti-neutrino flavor state  $|\bar{\nu}_\mu\rangle$  relevant to accelerator experiments.

In Fig. 9, the comparison illustrates  $\tau_{\text{QSL}}$  variation as a function of the propagation length  $L$  (km) for the initial state  $|\nu_\mu\rangle$  and  $|\bar{\nu}_\mu\rangle$  within both the normal hierarchy (NH) and inverted hierarchy (IH). Here,  $\tau_{\text{QSL}}$  for the initial muon neutrino state  $|\nu_\mu\rangle$  is characterized by a positive matter potential ( $+A_{\text{CC}}$ ) and a positive CP-violating phase ( $+\delta_{\text{CP}}$ ) in NH (magenta dotted line) and IH (red dot-dashed line). Conversely, for the muon anti-neutrino state  $|\bar{\nu}_\mu\rangle$ ,  $\tau_{\text{QSL}}$  is characterized by a negative matter potential ( $-A_{\text{CC}}$ ) and a negative CP-violating phase ( $-\delta_{\text{CP}}$ ) in NH (blue dashed line) and IH (green solid line). The difference in  $\tau_{\text{QSL}}$  between NH and IH for  $|\bar{\nu}_\mu\rangle$  is more significant compared to that observed for  $|\nu_\mu\rangle$ . To bring out the disparity in  $\tau_{\text{QSL}}$  between the muon and anti-muon states in NH and IH, for the selected mixing parameters, a zoomed-in figure (top left corner) within Fig. 9 is provided, focusing on the length scale range between 1100 km to 1300 km in the DUNE setup with an energy of 3.5 GeV. Moreover, under the constraint  $\tau_{\text{QSL}}/L < 1$ , in the NH scenario, a faster flavor evolution is estimated for both the initial states  $|\nu_\mu\rangle$  and  $|\bar{\nu}_\mu\rangle$ .

In the spirit of the two-flavor scenario, we now take up the case of entanglement in three-flavor neutrino oscillations in matter.

## VI. QUANTUM SPEED LIMIT TIME FOR ENTANGLEMENT IN THREE-FLAVOR NEUTRINO OSCILLATIONS IN MATTER

In the three-neutrino system, we map the three-flavor neutrino state to three-qubit states as [79]

$$\begin{aligned} |\nu_e\rangle &\equiv |1\rangle_e \otimes |0\rangle_\mu \otimes |0\rangle_\tau \equiv |100\rangle; \\ |\nu_\mu\rangle &\equiv |0\rangle_e \otimes |1\rangle_\mu \otimes |0\rangle_\tau \equiv |010\rangle; \\ |\nu_\tau\rangle &\equiv |0\rangle_e \otimes |0\rangle_\mu \otimes |1\rangle_\tau \equiv |001\rangle. \end{aligned} \quad (46)$$

Following eqn. (45) and eqn. (46), the time-evolved muon flavor neutrino states in matter can be represented in the three-qubit system as

$$|\nu_\mu(t)\rangle = \tilde{\mathcal{A}}_{\mu e}(t)|100\rangle + \tilde{\mathcal{A}}_{\mu\mu}(t)|010\rangle + \tilde{\mathcal{A}}_{\mu\tau}(t)|001\rangle, \quad (47)$$

where  $|\mathcal{A}_{\mu e}|^2 + |\mathcal{A}_{\mu\mu}|^2 + |\mathcal{A}_{\mu\tau}|^2 = 1$ . The corresponding density matrix  $\rho(t) = |\nu_\mu(t)\rangle\langle\nu_\mu(t)|$  in the standard basis  $|ijkl\rangle$ , where each index takes the values 0 and 1 is given by  $\rho(t) =$

$$\begin{pmatrix} 0 & 0 & 0 & 0 & 0 & 0 & 0 & 0 \\ 0 & 0 & 0 & 0 & 0 & 0 & 0 & 0 \\ 0 & 0 & 0 & 0 & 0 & 0 & 0 & 0 \\ 0 & 0 & 0 & |\tilde{\mathcal{A}}_{\mu e}(t)|^2 & \tilde{\mathcal{A}}_{\mu e}(t)\tilde{\mathcal{A}}_{\mu\mu}^*(t) & \tilde{\mathcal{A}}_{\mu e}(t)\tilde{\mathcal{A}}_{\mu\tau}^*(t) & 0 & 0 \\ 0 & 0 & 0 & 0 & 0 & 0 & 0 & 0 \\ 0 & 0 & 0 & \tilde{\mathcal{A}}_{\mu\mu}(t)\tilde{\mathcal{A}}_{\mu e}^*(t) & 0 & |\tilde{\mathcal{A}}_{\mu\mu}(t)|^2 & \tilde{\mathcal{A}}_{\mu\mu}(t)\tilde{\mathcal{A}}_{\mu\tau}^*(t) & 0 \\ 0 & 0 & 0 & \tilde{\mathcal{A}}_{\mu\tau}(t)\tilde{\mathcal{A}}_{\mu e}^*(t) & \tilde{\mathcal{A}}_{\mu\tau}(t)\tilde{\mathcal{A}}_{\mu\mu}^*(t) & |\tilde{\mathcal{A}}_{\mu\tau}(t)|^2 & 0 & 0 \\ 0 & 0 & 0 & 0 & 0 & 0 & 0 & 0 \end{pmatrix}. \quad (48)$$

Here  $\rho = \rho^2$  and  $\text{Tr}(\rho^2) = 1$ , i.e., a pure state. However, the reduced density matrix of the state  $\rho$  (by tracing over the other qubit(s)) denoted by  $\rho_{\mu e}(t) = \text{Tr}_{(\tau)}(\rho(t))$  and  $\rho_\tau(t) = \text{Tr}_{(\mu e)}(\rho(t))$

represent mixed states as  $\text{Tr}(\rho_{\mu e}^2(t)) < 1$  and  $\text{Tr}(\rho_\tau^2(t)) < 1$ . Thus, the reduced states  $\rho_{\mu e}(t)$  and  $\rho_\tau(t)$  provide an example of two subsystems of a bipartite quantum system  $\rho(t)$  in the framework of three-qubit mode (flavor) states. Treating one flavor mode as one part of the bipartite system  $\rho(t)$  (e.g.,  $\tau$ ) and the other as the remaining part (e.g.,  $\mu e$ ), the eigenvalues of the reduced state  $\rho_{\mu e}(t)$  are

$$\xi_1(t) = \xi_2(t) = 0; \quad \xi_3(t) = |\mathcal{A}_{\mu\mu}|^2; \quad \text{and} \quad \xi_4(t) = |\mathcal{A}_{\mu e}|^2 + |\mathcal{A}_{\mu\tau}|^2; \quad (49)$$

where,  $\xi_3(t) + \xi_4(t) = 1$ . Using the two nonzero eigenvalues, the bipartite entanglements measures such as entanglement entropy (eqn. (5)) and capacity of entanglement (eqn. (7)), can be calculated for the time-evolved muon flavor neutrino state  $|\nu_\mu(t)\rangle$  in matter as

$$S_{EE}(\rho_{\mu e}(t)) = -\xi_3(t) \log_2 \xi_3(t) - \xi_4(t) \log_2 \xi_4(t), \quad (50)$$

and

$$\begin{aligned} C_E(\rho_{\mu e}(t)) &= -\xi_3(t) \log_2^2 \xi_3(t) - \xi_4(t) \log_2^2 \xi_4(t) \\ &\quad - (-\xi_3(t) \log_2 \xi_3(t) - \xi_4(t) \log_2 \xi_4(t))^2, \end{aligned} \quad (51)$$

respectively. In a manner akin to the two-flavor neutrino oscillation in matter (as demonstrated in eqns. (42) and (43)), the two bipartite entanglement measures  $S_{EE}(\rho_{\mu e}(t))$  and  $C_E(\rho_{\mu e}(t))$  given in eqns. (50) and (51) for the three-flavor neutrino oscillation in a constant matter background can likewise be elucidated in terms of neutrino transition probabilities.

In the ultra-relativistic limit, Figs. (10a, 10c, and 10e) illustrate  $S_{EE}(\rho_{\mu e}(t))$  and  $C_E(\rho_{\mu e}(t))$  for the initial state  $|\nu_\mu\rangle$  in matter as a function of propagation length  $L$ (km), for T2K, NOvA and DUNE, respectively. The length scales and energies used correspond to T2K ( $L \approx 295$  km,  $E \approx 1$  GeV), NOvA ( $L \approx 800$  km,  $E \approx 4$  GeV), and DUNE ( $L \approx 1300$  km,  $E \approx 3.5$  GeV), respectively, considering two distinct CP violation phases:  $\delta_{\text{CP}} = 197^\circ$  in NH scenario and  $\delta_{\text{CP}} = 286^\circ$  in the IH scenario. By using the mixing parameters and mass-squared differences mentioned in Tables II and III, it is observed that for  $L > 0$ , entanglement measures  $S_{EE}(\rho_{\mu e}(t)) \neq 0$  and  $C_E(\rho_{\mu e}(t)) \neq 0$ . This suggests that the state  $|\nu_\mu(t)\rangle$  can be considered to be a bipartite pure entangled state in both NH and IH, with  $\delta_{\text{CP}}$  taken into account. In Fig. 10a, for the initial state  $|\nu_\mu\rangle$ ,  $S_{EE}$  monotonically increases in both NH (green solid line) and IH (red dot-dashed line) and approximately coincide within the range of propagation length  $L \approx 250$  km, for the  $\delta_{\text{CP}}$  chosen. Consequently,  $C_E$  also approximately coincides in NH (blue dotted line) and IH (magenta dashed line) while taking into account  $\delta_{\text{CP}}$  for the state  $|\nu_\mu(t)\rangle$ . This analysis indicates that T2K is unable to discern between the entanglement entropy for the initial state  $|\nu_\mu\rangle$  in NH and IH with  $\delta_{\text{CP}}$  under constant matter potential. However, in Fig. 10c, it is evident that NOvA's length scale and energy are able to capture the difference between the entanglement entropy  $S_{EE}$  in NH (green solid line) and IH (red dot-dashed line), with the chosen  $\delta_{\text{CP}}$ . Subsequently, a small difference between NH (blue dotted line) and IH (magenta dashed line) is observed for the capacity of entanglement  $C_E$ . At  $L \approx 800$ km, a separation in entanglement entropy  $S_{EE}$  is observed between the IH

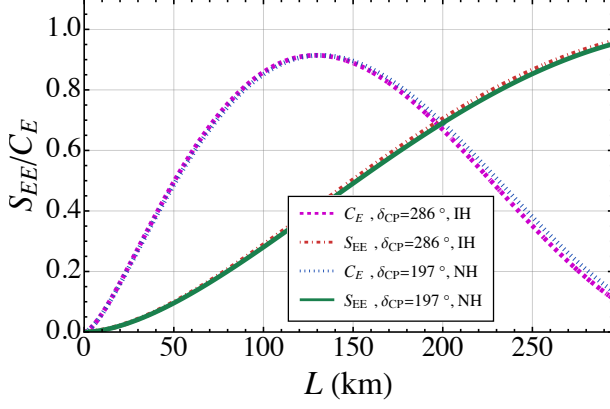
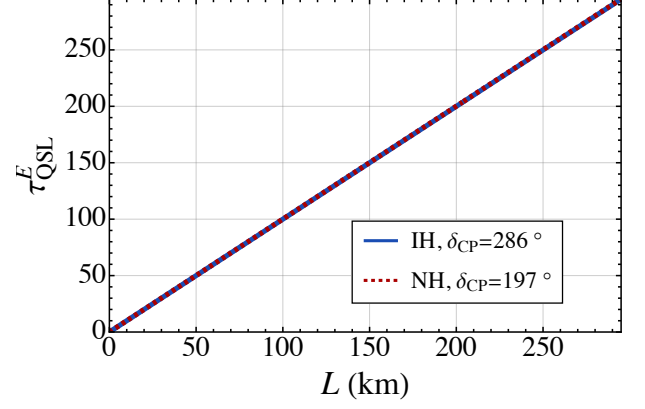
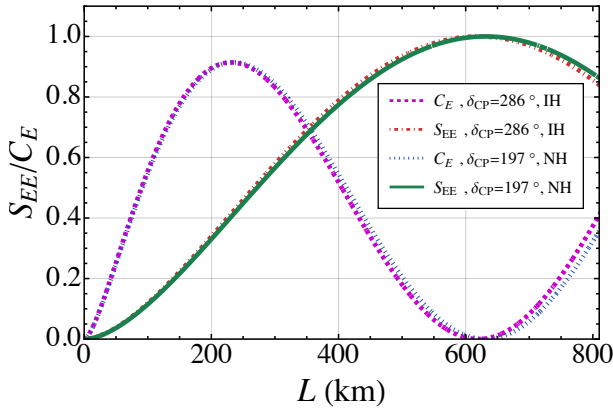
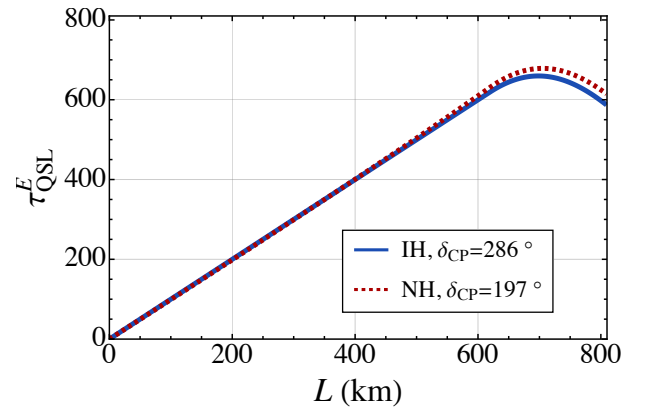
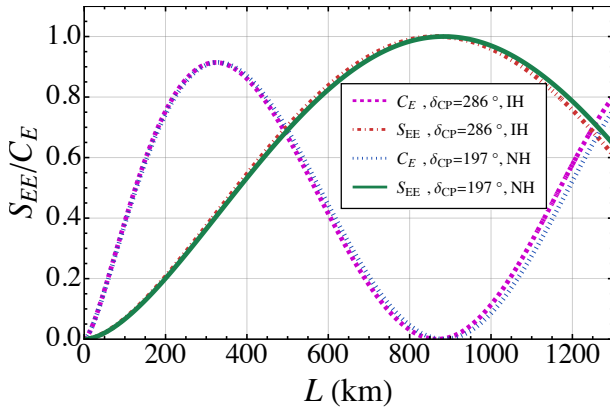
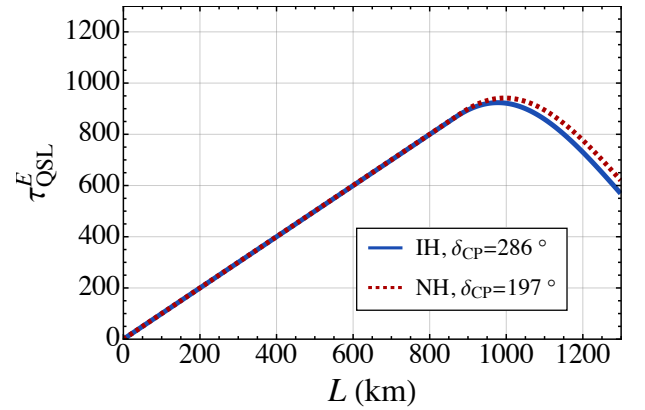
(a) T2K,  $\delta_{CP} = 197^\circ$  (NH),  $\delta_{CP} = 286^\circ$  (IH)(b) T2K,  $\delta_{CP} = 197^\circ$  (NH),  $\delta_{CP} = 286^\circ$  (IH)(c) NOvA,  $\delta_{CP} = 197^\circ$  (NH),  $\delta_{CP} = 286^\circ$  (IH)(d) NOvA,  $\delta_{CP} = 197^\circ$  (NH),  $\delta_{CP} = 286^\circ$  (IH)(e) DUNE,  $\delta_{CP} = 197^\circ$  (NH),  $\delta_{CP} = 286^\circ$  (IH)(f) DUNE,  $\delta_{CP} = 197^\circ$  (NH),  $\delta_{CP} = 286^\circ$  (IH)

FIG. 10: For three-flavor neutrino oscillations, Figs. 10a, 10c, and 10e depict entanglement entropy ( $S_{EE}(\rho_{\mu e}(t))$ ) and capacity of entanglement ( $C_E(\rho_{\mu e}(t))$ ) for the initial state  $|\nu_\mu\rangle$  in matter as a function of propagation length  $L$  (km) in both NH ( $\delta_{CP} = 197^\circ$ ) and IH ( $\delta_{CP} = 286^\circ$ ) using the length scales and energies corresponding to T2K, NOvA, and DUNE, respectively. Furthermore, we compare the QSL time  $\tau_{QSL}^E$  versus  $L$  (km) for the initial state  $|\nu_\mu\rangle$  in matter in NH ( $\delta_{CP} = 197^\circ$ ) and IH ( $\delta_{CP} = 286^\circ$ ). This comparison is illustrated in Figs. 10b, 10d, and 10f using the length scale and energy from T2K, NOvA, and DUNE, respectively. The various neutrino mixing parameters used are taken from Tables II for NH and III for IH along with their corresponding  $1\sigma$  errors (90% CL).

(red dot-dashed line) and the NH (green solid line), allowing them to be discerned. In Fig. 10e, the analysis using DUNE's length scale and energy reveals a significant split in  $S_{EE}$  between NH (green solid line) and IH (red dot-dashed line). At  $L \approx 1300$  km, more suppression of entanglement is observed in the IH. Consequently, at the same length, the capacity of entanglement  $C_E$  increases in the IH (magenta dashed line) compared to the NH (blue dotted line).

Moreover, for the state  $|\nu_\mu(t)\rangle$  in matter, we determine the variance in the driving Hamiltonian  $\Delta H_M$  (using eqn. (19)). Subsequently, applying eqns. (50) and (51) in eqn. (6) enables us to numerically compute the QSL time for entanglement entropy  $\tau_{\text{QSL}}^E$  of the state  $|\nu_\mu(t)\rangle$  in both NH and IH scenarios, with their respective CP violation phases. In Fig. 10b, it is observed that  $\tau_{\text{QSL}}^E$  for the initial state  $|\nu_\mu\rangle$  as a function of propagation length  $L$  (km) in NH (red dotted line) and in IH (blue solid line) with their respective CP violation phases coincide using the T2K length scale and energy. This leads to the time-bound condition  $\tau_{\text{QSL}}^E/L = 1$ . The result shows that the evolution speed of  $|\nu_\mu(t)\rangle$  has already reached its maximum in both NH and IH at  $L \approx 280$  km, and therefore T2K fails to capture any differences between the dynamic evolution of an entangled muon flavor neutrino state for speedup in NH and IH. In Fig. 10d, employing NOvA's length scale and energy, the plot of  $\tau_{\text{QSL}}^E$  vs  $L$  (km) demonstrates a slight disparity between the NH (red dotted line) and IH (blue solid line) scenarios, taking into account  $\delta_{\text{CP}}$ . Under the constraint  $\tau_{\text{QSL}}^E/L < 1$ , for the initial state  $|\nu_\mu\rangle$  in matter, a rapid suppression of entanglement is observed in the IH (blue solid line) compared to the NH (red dotted line) within the range of  $\delta_{\text{CP}}$ . However, at DUNE's length scale and energy, Fig. 10f illustrates a significantly greater disparity between  $\tau_{\text{QSL}}^E$  vs  $L$  (km) in the NH (red dotted line) and IH (blue solid line). It is evident that a much more rapid suppression of entanglement is observable in the IH (blue solid line) compared to the NH (red dotted line) within the range of  $\delta_{\text{CP}}$ . Alternatively, one can say that within the framework of three-flavor neutrino oscillations in matter, for the initial state  $|\nu_\mu\rangle$ , faster growth of entanglement is observed in DUNE under the assumption of NH. Therefore, DUNE exhibits higher sensitivity in observing  $\tau_{\text{QSL}}^E$  compared to T2K and NOvA.

## VII. DISCUSSIONS AND CONCLUSIONS

We have studied CP violation and the mass hierarchy problem of neutrino oscillations in matter, employing the QSL time as a key analytical tool. As a precursor to the three-flavor oscillations, the QSL time for two-flavor neutrino oscillations in matter has been initially analyzed. Our findings have revealed that rapid transitions of flavor neutrinos occur from initial to final states as the neutrino potential shifts from vacuum to a constant earth-matter potential. Furthermore, we have explored two bipartite entanglement measures: entanglement entropy and capacity of entanglement—quantified in terms of two-flavor neutrino transition probabilities in matter, which are measurable quantities in neutrino experiments. The non-zero values of these entanglement measures indicate a bi-

partite pure entangled system during two-flavor neutrino oscillations in vacuum as well as in matter. For the initial electron flavor neutrino state evolution, the QSL time for entanglement entropy indicates rapid suppression of entanglement when neutrinos begin oscillating in constant earth-matter instead of vacuum.

In order to probe the impact of CP violation and the mass hierarchy problem of neutrino oscillations in matter, we have extended our analysis to three-flavor neutrino oscillations in the presence of a constant earth-matter potential with CP violation phases, considering two cases of neutrino mass hierarchy: Normal Hierarchy (NH) and Inverted Hierarchy (IH). We have focused on the initial muon flavor neutrino state evolution and used the length scale and energy data from Long-Baseline neutrino experiments T2K, NOvA, and DUNE. Our results have revealed discrepancies in the QSL time, for the initial muon flavor neutrino state evolution, between NH and IH in the presence of their corresponding CP violating phases across these experiments. Notably, a faster evolution of the initial muon flavor neutrino state in matter is achievable in NH taking into account CP violation phases in all three experiments. Moreover, at DUNE's length scale and energy, we have observed faster flavor state evolution for both the initial muon neutrino and muon anti-neutrino flavor states in the NH scenario.

In the three-flavor oscillations scenario, entanglement entropy and capacity of entanglement could be expressed in terms of three-flavor transition probabilities for the initial muon-flavor neutrino state. While there are no discrepancies in the entanglement entropy found as CP violation phases increase from low to high values in both NH and IH using T2K data, discrepancies are observed when we used NOvA and DUNE data. Specifically, a greater decrease in entanglement entropy has been observed at DUNE's length scale and energy for the initial muon flavour neutrino state evolution in the presence of a constant earth-matter background in IH with CP violation.

Further, for the initial muon flavor neutrino state evolution, the QSL time for entanglement entropy has been numerically computed in NH and IH with CP violation phases using T2K, NOvA, and DUNE length scales and energies. T2K fails to capture any differences in the QSL time for entanglement between NH and IH in the presence of CP violation phase. However, NOvA and DUNE have shown sensitivity in capturing these differences. Faster growth of entanglement, for the initial muon flavor neutrino state evolution in matter, has been observed in NH, in the presence of a significant CP violation phase, at DUNE's length scale and energy. These findings could help in ascertaining the role of CP violation and determination of the mass hierarchy in neutrino oscillations.

## ACKNOWLEDGMENTS

We thank Banibrata Mukhopadhyay, Ranjan Laha, and Brij Mohan for their fruitful discussions and insightful input. Subhadip Bouri acknowledges the Council of Scientific and Industrial Research (CSIR), Government of India, for support-

ing his research under the CSIR Junior/Senior Research Fellowship program through grant no. 09/0079(15488)/2022-

EMR-I. AKJ and SB would like to acknowledge the project funded by SERB, India, with Ref. No. CRG/2022/003460, for supporting this research.

- 
- [1] H. P. Robertson, The uncertainty principle, *Phys. Rev.* **34**, 163 (1929).
- [2] L. Maccone and A. K. Pati, Stronger uncertainty relations for all incompatible observables, *Phys. Rev. Lett.* **113**, 260401 (2014).
- [3] L. Mandelstam and I. Tamm, The uncertainty relation between energy and time in non-relativistic quantum mechanics, in *Selected Papers*, edited by B. M. Bolotovskii, V. Y. Frenkel, and R. Peierls (Springer Berlin Heidelberg, Berlin, Heidelberg, 1991) pp. 115–123.
- [4] N. Margolus and L. B. Levitin, The maximum speed of dynamical evolution, *Physica D: Nonlinear Phenomena* **120**, 188 (1998), proceedings of the Fourth Workshop on Physics and Consumption.
- [5] L. B. Levitin and T. Toffoli, Fundamental limit on the rate of quantum dynamics: The unified bound is tight, *Phys. Rev. Lett.* **103**, 160502 (2009).
- [6] J. Anandan and Y. Aharonov, Geometry of quantum evolution, *Phys. Rev. Lett.* **65**, 1697 (1990).
- [7] A. K. Pati, Relation between “phases” and “distance” in quantum evolution, *Physics Letters A* **159**, 105 (1991).
- [8] J. S. Anandan and A. K. Pati, Geometry of the Josephson effect, *Physics Letters A* **231**, 29 (1997).
- [9] A. K. Pati, New derivation of the geometric phase, *Physics Letters A* **202**, 40 (1995).
- [10] V. Giovannetti, S. Lloyd, and L. Maccone, Quantum limits to dynamical evolution, *Phys. Rev. A* **67**, 052109 (2003), arXiv:quant-ph/0210197 [quant-ph].
- [11] S. Deffner and E. Lutz, Energy–time uncertainty relation for driven quantum systems, *Journal of Physics A: Mathematical and Theoretical* **46**, 335302 (2013).
- [12] S. Deffner and S. Campbell, Quantum speed limits: from Heisenberg’s uncertainty principle to optimal quantum control, *J. Phys. A* **50**, 453001 (2017), arXiv:1705.08023 [quant-ph].
- [13] D. Thakuria, A. Srivastav, B. Mohan, A. Kumari, and A. K. Pati, Generalised quantum speed limit for arbitrary time-continuous evolution, *Journal of Physics A Mathematical General* **57**, 025302 (2024), arXiv:2207.04124 [quant-ph].
- [14] S. Deffner and E. Lutz, Nonequilibrium Entropy Production for Open Quantum Systems, *Phys. Rev. Lett.* **107**, 140404 (2011), arXiv:1103.4775 [cond-mat.stat-mech].
- [15] R. Baruah, K. G. Paulson, and S. Banerjee, Phase Covariant Channel: Quantum Speed Limit of Evolution, *Annalen Phys.* **535**, 2200199 (2023), arXiv:2204.08149 [quant-ph].
- [16] S. Ashhab, P. C. de Groot, and F. Nori, Speed limits for quantum gates in multiqubit systems, *Phys. Rev. A* **85**, 052327 (2012).
- [17] S. Aggarwal, S. Banerjee, A. Ghosh, and B. Mukhopadhyay, Non-uniform magnetic field as a booster for quantum speed limit: faster quantum information processing, *New J. Phys.* **24**, 085001 (2022), arXiv:2112.04519 [quant-ph].
- [18] J. D. Bekenstein, Energy Cost of Information Transfer, *Phys. Rev. Lett.* **46**, 623 (1981).
- [19] K. G. Paulson, S. Banerjee, and R. Srikanth, The effect of quantum memory on quantum speed limit time for CP-(in)divisible channels, *Quant. Inf. Proc.* **21**, 335 (2022), arXiv:2107.03306 [quant-ph].
- [20] K. G. Paulson and S. Banerjee, Quantum speed limit time: role of coherence, *J. Phys. A* **55**, 505302 (2022), arXiv:2202.08078 [quant-ph].
- [21] D. Tiwari, K. G. Paulson, and S. Banerjee, Quantum Correlations and Speed Limit of Central Spin Systems, *Annalen Phys.* **535**, 2200452 (2023), arXiv:2205.13195 [quant-ph].
- [22] S. Lloyd, Ultimate physical limits to computation, *Nature (London)* **406**, 1047 (2000), arXiv:quant-ph/9908043 [quant-ph].
- [23] M. Zwiernik, C. A. Pérez-Delgado, and P. Kok, General Optimality of the Heisenberg Limit for Quantum Metrology, *Phys. Rev. Lett.* **105**, 180402 (2010), arXiv:1004.3944 [quant-ph].
- [24] V. Giovannetti, S. Lloyd, and L. Maccone, Advances in quantum metrology, *Nature Photonics* **5**, 222 (2011), arXiv:1102.2318 [quant-ph].
- [25] A. d. Campo, J. Gould, and M. Paternostro, More bang for your buck: Super-adiabatic quantum engines, *Scientific Reports* **4**, 10.1038/srep06208 (2014).
- [26] K. Funo, N. Shiraishi, and K. Saito, Speed limit for open quantum systems, *New Journal of Physics* **21**, 013006 (2019), arXiv:1810.03011 [quant-ph].
- [27] T. Caneva, M. Murphy, T. Calarco, R. Fazio, S. Montangero, V. Giovannetti, and G. E. Santoro, Optimal Control at the Quantum Speed Limit, *Phys. Rev. Lett.* **103**, 240501 (2009), arXiv:0902.4193 [quant-ph].
- [28] M. Murphy, S. Montangero, V. Giovannetti, and T. Calarco, Communication at the quantum speed limit along a spin chain, *Phys. Rev. A* **82**, 022318 (2010), arXiv:1004.3445 [quant-ph].
- [29] F. Campaioli, F. A. Pollock, and S. Vinjanampathy, Quantum batteries, in *Thermodynamics in the Quantum Regime: Fundamental Aspects and New Directions*, edited by F. Binder, L. A. Correa, C. Gogolin, J. Anders, and G. Adesso (Springer International Publishing, Cham, 2018) pp. 207–225.
- [30] S. Julià-Farré, T. Salamon, A. Riera, M. N. Bera, and M. Lewenstein, Bounds on the capacity and power of quantum batteries, *Physical Review Research* **2**, 023113 (2020).
- [31] B. Mohan and A. K. Pati, Reverse quantum speed limit: How slowly a quantum battery can discharge, *Phys. Rev. A* **104**, 042209 (2021), arXiv:2006.14523 [quant-ph].
- [32] B. Mohan and A. K. Pati, Quantum speed limits for observables, *Phys. Rev. A* **106**, 042436 (2022), arXiv:2112.13789 [quant-ph].
- [33] K. Liegener and L. Rudnicki, Quantum speed limit and stability of coherent states in quantum gravity, *Class. Quant. Grav.* **39**, 12LT01 (2022), arXiv:2112.01597 [gr-qc].
- [34] Z.-D. Wei, W. Han, Y.-J. Zhang, S.-J. Du, Y.-J. Xia, and H. Fan, Non-Markovian speedup dynamics of a photon induced by gravitational redshift, *Phys. Rev. D* **108**, 126011 (2023).
- [35] Q. Wang, K. Xu, W.-B. Yan, Y.-J. Zhang, Z.-X. Man, Y.-J. Xia, and H. Fan, Control of quantum dynamics: non-Markovianity and speedup of a massive particle evolution due to gravity, *Eur. Phys. J. C* **82**, 729 (2022).

- [36] Y. Maleki and A. Maleki, Speed limit of quantum dynamics near the event horizon of black holes, *Phys. Lett. B* **810**, 135700 (2020), [arXiv:1906.10894 \[hep-th\]](#).
- [37] S. Banerjee, A. K. Alok, and R. MacKenzie, Quantum correlations in B and K meson systems, *Eur. Phys. J. Plus* **131**, 129 (2016), [arXiv:1409.1034 \[hep-ph\]](#).
- [38] J. Naikoo, A. K. Alok, and S. Banerjee, Study of temporal quantum correlations in decohering B and K meson systems, *Phys. Rev. D* **97**, 053008 (2018), [arXiv:1802.04265 \[hep-ph\]](#).
- [39] S. Banerjee and K. G. Paulson, Quantum speed of evolution of neutral mesons, *Eur. Phys. J. Plus* **138**, 597 (2023), [arXiv:2206.13938 \[hep-ph\]](#).
- [40] F. Khan and J. Dajka, Geometric speed limit of neutrino oscillation, *Quant. Inf. Proc.* **20**, 193 (2021).
- [41] C. Giunti and C. W. Kim, *Fundamentals of Neutrino Physics and Astrophysics* (Oxford University Press, 2007).
- [42] Y. Fukuda *et al.* (Super-Kamiokande), Evidence for oscillation of atmospheric neutrinos, *Phys. Rev. Lett.* **81**, 1562 (1998), [arXiv:hep-ex/9807003](#).
- [43] T. Kajita, Nobel Lecture: Discovery of atmospheric neutrino oscillations\*, *Reviews of Modern Physics* **88**, 030501 (2016).
- [44] A. B. McDonald, Nobel lecture: the sudbury neutrino observatory: observation of flavor change for solar neutrinos, *Reviews of Modern Physics* **88**, 030502 (2016).
- [45] B. Pontecorvo, Mesonium and anti-mesonium, *Sov. Phys. JETP* **6**, 429 (1957).
- [46] B. Pontecorvo, Inverse beta processes and nonconservation of lepton charge, *Zh. Eksp. Teor. Fiz.* **34**, 247 (1957).
- [47] B. Pontecorvo, Neutrino Experiments and the Problem of Conservation of Leptonic Charge, *Zh. Eksp. Teor. Fiz.* **53**, 1717 (1967).
- [48] S. M. Bilenky and B. Pontecorvo, Lepton Mixing and Neutrino Oscillations, *Phys. Rept.* **41**, 225 (1978).
- [49] S. M. Bilenky, The History of neutrino oscillations, *Phys. Scripta T* **121**, 17 (2005), [arXiv:hep-ph/0410090](#).
- [50] C. Giganti, S. Lavignac, and M. Zito, Neutrino oscillations: The rise of the PMNS paradigm, *Prog. Part. Nucl. Phys.* **98**, 1 (2018), [arXiv:1710.00715 \[hep-ex\]](#).
- [51] Z. Maki, M. Nakagawa, and S. Sakata, Remarks on the unified model of elementary particles, *Prog. Theor. Phys.* **28**, 870 (1962).
- [52] J. Schechter and J. W. F. Valle, Neutrino-oscillation thought experiment, *Phys. Rev. D* **23**, 1666 (1981).
- [53] K. Abe *et al.* (T2K), Constraint on the matter–antimatter symmetry-violating phase in neutrino oscillations, *Nature* **580**, 339 (2020), [Erratum: *Nature* **583**, E16 (2020)], [arXiv:1910.03887 \[hep-ex\]](#).
- [54] H. Minakata and H. Nunokawa, CP violation versus the matter effect in long-baseline neutrino oscillation experiments, *Phys. Rev. D* **57**, 4403 (1998), [arXiv:hep-ph/9705208 \[hep-ph\]](#).
- [55] I. Y. Kobzarev, B. V. Martemyanov, L. B. Okun, and M. G. Shchepkin, Sum Rules for Neutrino Oscillations, *Sov. J. Nucl. Phys.* **35**, 708 (1982).
- [56] A. Gando *et al.* (KamLAND), Reactor On-Off Antineutrino Measurement with KamLAND, *Phys. Rev. D* **88**, 033001 (2013), [arXiv:1303.4667 \[hep-ex\]](#).
- [57] P. B. Denton, M. Friend, M. D. Messier, H. A. Tanaka, S. Böser, J. a. A. B. Coelho, M. Perrin-Terrin, and T. Stuttard, Snowmass Neutrino Frontier: NF01 Topical Group Report on Three-Flavor Neutrino Oscillations, (2022), [arXiv:2212.00809 \[hep-ph\]](#).
- [58] F. P. An *et al.* (Daya Bay), Spectral measurement of electron antineutrino oscillation amplitude and frequency at Daya Bay, *Phys. Rev. Lett.* **112**, 061801 (2014), [arXiv:1310.6732 \[hep-ex\]](#).
- [59] G. Bak *et al.* (RENO), Measurement of Reactor Antineutrino Oscillation Amplitude and Frequency at RENO, *Phys. Rev. Lett.* **121**, 201801 (2018), [arXiv:1806.00248 \[hep-ex\]](#).
- [60] H. de Kerret *et al.* (Double Chooz), Double Chooz  $\theta_{13}$  measurement via total neutron capture detection, *Nature Phys.* **16**, 558 (2020), [arXiv:1901.09445 \[hep-ex\]](#).
- [61] F. Di Lodovico, The Hyper-Kamiokande Experiment, *PoS FPCP2015*, 038 (2015).
- [62] V. A. Kudryavtsev and for the DUNE Collaboration, Underground physics with dune, *Journal of Physics: Conference Series* **718**, 062032 (2016).
- [63] T. Ohlsson and H. Snellman, Three flavor neutrino oscillations in matter, *J. Math. Phys.* **41**, 2768 (2000), [Erratum: *J. Math. Phys.* **42**, 2345 (2001)], [arXiv:hep-ph/9910546](#).
- [64] T. Ohlsson and H. Snellman, Neutrino oscillations with three flavors in matter: Applications to neutrinos traversing the Earth, *Phys. Lett. B* **474**, 153 (2000), [Erratum: *Phys. Lett. B* **480**, 419–419 (2000)], [arXiv:hep-ph/9912295](#).
- [65] P. B. Denton, H. Minakata, and S. J. Parke, Compact perturbative expressions for neutrino oscillations in matter, *Journal of High Energy Physics* **2016**, 51 (2016), [arXiv:1604.08167 \[hep-ph\]](#).
- [66] G. Barenboim, P. B. Denton, S. J. Parke, and C. A. Ternes, Neutrino oscillation probabilities through the looking glass, *Physics Letters B* **791**, 351 (2019), [arXiv:1902.00517 \[hep-ph\]](#).
- [67] L. Wolfenstein, Neutrino oscillations in matter, *Phys. Rev. D* **17**, 2369 (1978).
- [68] M. A. Nielsen and I. L. Chuang, *Quantum Computation and Quantum Information: 10th Anniversary Edition* (Cambridge University Press, 2010).
- [69] M. Blasone, F. Dell’Anno, S. De Siena, and F. Illuminati, Entanglement in neutrino oscillations, *EPL* **85**, 50002 (2009), [arXiv:0707.4476 \[hep-ph\]](#).
- [70] M. Blasone, F. Dell’Anno, S. De Siena, and F. Illuminati, Neutrino flavor entanglement, *Nuclear Physics B - Proceedings Supplements* **237-238**, 320 (2013), proceedings of the Neutrino Oscillation Workshop.
- [71] M. Blasone, F. Dell’Anno, S. de Siena, M. di Mauro, and F. Illuminati, Multipartite entangled states in particle mixing, *Phys. Rev. D* **77**, 096002 (2008), [arXiv:0711.2268 \[quant-ph\]](#).
- [72] M. Blasone, F. Dell’Anno, S. de Siena, and F. Illuminati, Hierarchies of geometric entanglement, *Phys. Rev. A* **77**, 062304 (2008), [arXiv:0712.4085 \[quant-ph\]](#).
- [73] S. Banerjee, A. K. Alok, R. Srikanth, and B. C. Hiesmayr, A quantum information theoretic analysis of three flavor neutrino oscillations, *Eur. Phys. J. C* **75**, 487 (2015), [arXiv:1508.03480 \[hep-ph\]](#).
- [74] A. K. Alok, S. Banerjee, and S. U. Sankar, Quantum correlations in terms of neutrino oscillation probabilities, *Nucl. Phys. B* **909**, 65 (2016), [arXiv:1411.5536 \[hep-ph\]](#).
- [75] K. Dixit, A. K. Alok, S. Banerjee, and D. Kumar, Geometric phase and neutrino mass hierarchy problem, *J. Phys. G* **45**, 085002 (2018), [arXiv:1703.09894 \[hep-ph\]](#).
- [76] K. Dixit, J. Naikoo, S. Banerjee, and A. K. Alok, Quantum correlations and the neutrino mass degeneracy problem, *Eur. Phys. J. C* **78**, 914 (2018), [arXiv:1807.01546 \[hep-ph\]](#).
- [77] K. Dixit and A. Kumar Alok, New physics effects on quantum coherence in neutrino oscillations, *Eur. Phys. J. Plus* **136**, 334 (2021), [arXiv:1909.04887 \[hep-ph\]](#).
- [78] K. Dixit and A. K. Alok, Effects of Nonstandard Interactions on Coherence in Neutrino Oscillations, *Springer Proc. Phys.* **248**, 343 (2020).

- [79] A. Kumar Jha, S. Mukherjee, and B. A. Bambah, Tri-Partite entanglement in Neutrino Oscillations, *Mod. Phys. Lett. A* **36**, 2150056 (2021), arXiv:2004.14853 [hep-ph].
- [80] B. Yadav, T. Sarkar, K. Dixit, and A. K. Alok, Can NSI affect non-local correlations in neutrino oscillations?, *Eur. Phys. J. C* **82**, 446 (2022), arXiv:2201.05580 [hep-ph].
- [81] Y.-W. Li, L.-J. Li, X.-K. Song, D. Wang, and L. Ye, Geuine tripartite entanglement in three-flavor neutrino oscillations, *Eur. Phys. J. C* **82**, 799 (2022), arXiv:2205.11058 [quant-ph].
- [82] G.-J. Wang, Y.-W. Li, L.-J. Li, X.-K. Song, and D. Wang, Monogamy properties of quantum correlations in neutrino oscillations, *European Physical Journal C* **83**, 801 (2023).
- [83] V. Bittencourt, M. Blasone, S. De Siena, and C. Matrella, Quantifying quantumness in three-flavor neutrino oscillations, (2023), arXiv:2305.06095 [quant-ph].
- [84] M. Blasone, S. De Siena, and C. Matrella, Complete complementarity relations and quantifiers of quantum correlations in neutrino oscillations, *PoS CORFU2022*, 044 (2023).
- [85] G. M. Quinta, A. Sousa, and Y. Omar, Predicting leptonic CP violation via minimization of neutrino entanglement, (2022), arXiv:2207.03303 [hep-ph].
- [86] A. K. Jha, A. Chatla, and B. A. Bambah, Neutrinos as qubits and qutrits, *Eur. Phys. J. Plus* **139**, 68 (2024), arXiv:2203.13485 [hep-ph].
- [87] K. Dixit, S. S. Haque, and S. Razzaque, Quantum spread complexity in neutrino oscillations, *Eur. Phys. J. C* **84**, 260 (2024), arXiv:2305.17025 [hep-ph].
- [88] L. Konwar and B. Yadav, NSI effects on tripartite entanglement in neutrino oscillations, (2024), arXiv:2402.09952 [hep-ph].
- [89] M. Blasone, F. Dell'Anno, S. De Siena, and F. Illuminati, Flavor entanglement in neutrino oscillations in the wave packet description, *EPL (Europhysics Letters)* **112**, 20007 (2015), arXiv:1510.06761 [quant-ph].
- [90] M. Blasone, S. De Siena, and C. Matrella, Wave packet approach to quantum correlations in neutrino oscillations, *Eur. Phys. J. C* **81**, 660 (2021), arXiv:2104.03166 [quant-ph].
- [91] M. Blasone, S. De Siena, and C. Matrella, Non-locality and entropic uncertainty relations in neutrino oscillations, *Eur. Phys. J. Plus* **137**, 1272 (2022), arXiv:2206.13218 [quant-ph].
- [92] Z. A. Ravari, M. M. Ettefaghi, and S. Miraboutalebi, Quantum coherence in neutrino oscillation in matter, *Eur. Phys. J. Plus* **137**, 488 (2022), arXiv:2204.12332 [quant-ph].
- [93] M. M. Ettefaghi and Z. A. Ravari, Quantum coherence and entanglement in neutral-current neutrino oscillation in matter, *Eur. Phys. J. C* **83**, 417 (2023), arXiv:2305.12194 [hep-ph].
- [94] J. A. Formaggio, D. I. Kaiser, M. M. Murskyj, and T. E. Weiss, Violation of the Leggett-Garg Inequality in Neutrino Oscillations, *Phys. Rev. Lett.* **117**, 050402 (2016), arXiv:1602.00041 [quant-ph].
- [95] J. Naikoo, A. K. Alok, S. Banerjee, and S. U. Sankar, Leggett-Garg inequality in the context of three flavor neutrino oscillation, *Phys. Rev. D* **99**, 095001 (2019), arXiv:1901.10859 [hep-ph].
- [96] J. Naikoo, A. K. Alok, S. Banerjee, S. Uma Sankar, G. Guarnieri, C. Schultze, and B. C. Hiesmayr, A quantum information theoretic quantity sensitive to the neutrino mass-hierarchy, *Nucl. Phys. B* **951**, 114872 (2020), arXiv:1710.05562 [hep-ph].
- [97] M. Blasone, F. Illuminati, L. Petruzzello, K. Simonov, and L. Smaldone, No-signaling-in-time as a condition for macro-realism: the case of neutrino oscillations, *Eur. Phys. J. C* **83**, 688 (2023), arXiv:2211.16931 [hep-th].
- [98] D. S. Chattopadhyay and A. Dighe, Quantum mismatch: A powerful measure of quantumness in neutrino oscillations, *Phys. Rev. D* **108**, 112013 (2023), arXiv:2304.02475 [hep-ph].
- [99] B. Soni, S. Shafaq, and P. Mehta, Distinguishing between Dirac and Majorana neutrinos using temporal correlations, (2023), arXiv:2307.04496 [hep-ph].
- [100] S. Shafaq and P. Mehta, Enhanced violation of Leggett–Garg inequality in three flavour neutrino oscillations via non-standard interactions, *J. Phys. G* **48**, 085002 (2021), arXiv:2009.12328 [hep-ph].
- [101] T. Sarkar and K. Dixit, Effects of nonstandard interaction on temporal and spatial correlations in neutrino oscillations, *Eur. Phys. J. C* **81**, 88 (2021), arXiv:2010.02175 [hep-ph].
- [102] X.-K. Song, Y. Huang, J. Ling, and M.-H. Yung, Quantifying quantum coherence in experimentally observed neutrino oscillations, *Phys. Rev. A* **98**, 050302 (2018), arXiv:1806.00715 [hep-ph].
- [103] K. Dixit, J. Naikoo, S. Banerjee, and A. Kumar Alok, Study of coherence and mixedness in meson and neutrino systems, *Eur. Phys. J. C* **79**, 96 (2019), arXiv:1809.09947 [hep-ph].
- [104] Y.-W. Li, L.-J. Li, X.-K. Song, and D. Wang, Trade-off relations of quantum resource theory in neutrino oscillations, *Eur. Phys. J. Plus* **137**, 1267 (2022), arXiv:2212.09320 [quant-ph].
- [105] C. A. Argüelles and B. J. P. Jones, Neutrino Oscillations in a Quantum Processor, *Phys. Rev. Research* **1**, 033176 (2019), arXiv:1904.10559 [quant-ph].
- [106] M. J. Molewski and B. J. P. Jones, Scalable qubit representations of neutrino mixing matrices, *Phys. Rev. D* **105**, 056024 (2022), arXiv:2111.05401 [quant-ph].
- [107] A. K. Jha and A. Chatla, Quantum studies of neutrinos on IBMQ processors, *Eur. Phys. J. ST* **231**, 141 (2022).
- [108] H. C. Nguyen, B. G. Bach, T. D. Nguyen, D. M. Tran, D. V. Nguyen, and H. Q. Nguyen, Simulating neutrino oscillations on a superconducting qutrit, *Phys. Rev. D* **108**, 023013 (2023), arXiv:2212.14170 [quant-ph].
- [109] B. Mohan, S. Das, and A. K. Pati, Quantum speed limits for information and coherence, *New J. Phys.* **24**, 065003 (2022), arXiv:2110.13193 [quant-ph].
- [110] V. Pandey, D. Shrimali, B. Mohan, S. Das, and A. K. Pati, Speed limits on correlations in bipartite quantum systems, *Phys. Rev. A* **107**, 052419 (2023), arXiv:2207.05645 [quant-ph].
- [111] S. Das, S. Khatri, G. Siopsis, and M. M. Wilde, Fundamental limits on quantum dynamics based on entropy change, *J. Math. Phys.* **59**, 012205 (2018), arXiv:1707.06584 [quant-ph].
- [112] D. Shrimali, S. Bhowmick, V. Pandey, and A. K. Pati, Capacity of entanglement for a nonlocal Hamiltonian, *Phys. Rev. A* **106**, 042419 (2022), arXiv:2207.11459 [quant-ph].
- [113] H. Li and F. D. M. Haldane, Entanglement Spectrum as a Generalization of Entanglement Entropy: Identification of Topological Order in Non-Abelian Fractional Quantum Hall Effect States, *Phys. Rev. Lett.* **101**, 010504 (2008), arXiv:0805.0332 [cond-mat.mes-hall].
- [114] J. De Boer, J. Järvelä, and E. Keski-Vakkuri, Aspects of capacity of entanglement, *Phys. Rev. D* **99**, 066012 (2019), arXiv:1807.07357 [hep-th].
- [115] H. Yao and X.-L. Qi, Entanglement Entropy and Entanglement Spectrum of the Kitaev Model, *Phys. Rev. Lett.* **105**, 080501 (2010), arXiv:1001.1165 [cond-mat.str-el].
- [116] E. Rrapaj, Exact solution of multiangle quantum many-body collective neutrino-flavor oscillations, *Phys. Rev. C* **101**, 065805 (2020), arXiv:1905.13335 [hep-ph].
- [117] B. Hall, A. Roggero, A. Baroni, and J. Carlson, Simulation of collective neutrino oscillations on a quantum computer, *Phys.*

- Rev. D **104**, 063009 (2021), arXiv:2102.12556 [quant-ph].
- [118] P. Siwach, A. M. Suliga, and A. B. Balantekin, Entanglement in three-flavor collective neutrino oscillations, *Phys. Rev. D* **107**, 023019 (2023), arXiv:2211.07678 [hep-ph].
- [119] T. K. Kuo and J. Pantaleone, Neutrino oscillations in matter, *Rev. Mod. Phys.* **61**, 937 (1989).
- [120] M. Blennow and A. Y. Smirnov, Neutrino propagation in matter, *Adv. High Energy Phys.* **2013**, 972485 (2013), arXiv:1306.2903 [hep-ph].
- [121] S. Parke, What is  $\Delta m_e^{e2}$ ?, *Phys. Rev. D* **93**, 053008 (2016), arXiv:1601.07464 [hep-ph].
- [122] I. Esteban, M. C. Gonzalez-Garcia, M. Maltoni, T. Schwetz, and A. Zhou, The fate of hints: updated global analysis of three-flavor neutrino oscillations, *JHEP* **09**, 178, arXiv:2007.14792 [hep-ph].
- [123] NuFIT, 5.2 (2022).
- [124] K. Abe *et al.* (T2K), Indication of Electron Neutrino Appearance from an Accelerator-produced Off-axis Muon Neutrino Beam, *Phys. Rev. Lett.* **107**, 041801 (2011), arXiv:1106.2822 [hep-ex].
- [125] D. S. Ayres *et al.* (NOvA), NOvA: Proposal to Build a 30 Kiloton Off-Axis Detector to Study  $\nu_\mu \rightarrow \nu_e$  Oscillations in the NuMI Beamline, (2004), arXiv:hep-ex/0503053.
- [126] B. Abi *et al.* (DUNE), Deep Underground Neutrino Experiment (DUNE), Far Detector Technical Design Report, Volume II: DUNE Physics, (2020), arXiv:2002.03005 [hep-ex].
- [127] C. Adams *et al.* (LBNE), The Long-Baseline Neutrino Experiment: Exploring Fundamental Symmetries of the Universe, in *Snowmass 2013: Workshop on Energy Frontier* (2013) arXiv:1307.7335 [hep-ex].
- [128] L. Wolfenstein, Oscillations Among Three Neutrino Types and CP Violation, *Phys. Rev. D* **18**, 958 (1978).
- [129] P. Langacker, Grand Unified Theories and Proton Decay, *Phys. Rept.* **72**, 185 (1981).
- [130] S. M. Bilenky and S. T. Petcov, Massive Neutrinos and Neutrino Oscillations, *Rev. Mod. Phys.* **59**, 671 (1987), [Erratum: *Rev. Mod. Phys.* **61**, 169 (1989), Erratum: *Rev. Mod. Phys.* **60**, 575–575 (1988)].
- [131] H. Nunokawa, S. J. Parke, and J. W. F. Valle, CP Violation and Neutrino Oscillations, *Prog. Part. Nucl. Phys.* **60**, 338 (2008), arXiv:0710.0554 [hep-ph].
- [132] G. C. Branco, L. Lavoura, and J. P. Silva, *CP Violation*, Vol. 103 (1999).
- [133] L. Canetti, M. Drewes, and M. Shaposhnikov, Matter and Antimatter in the Universe, *New J. Phys.* **14**, 095012 (2012), arXiv:1204.4186 [hep-ph].
- [134] A. Abada, S. Davidson, A. Ibarra, F. X. Josse-Michaux, M. Losada, and A. Riotto, Flavour Matters in Leptogenesis, *JHEP* **09**, 010, arXiv:hep-ph/0605281.
- [135] J. Burguet-Castell, M. B. Gavela, J. J. Gomez-Cadenas, P. Hernandez, and O. Mena, On the Measurement of leptonic CP violation, *Nucl. Phys. B* **608**, 301 (2001), arXiv:hep-ph/0103258.
- [136] W. Buchmuller, P. Di Bari, and M. Plumacher, The Neutrino mass window for baryogenesis, *Nucl. Phys. B* **665**, 445 (2003), arXiv:hep-ph/0302092.
- [137] V. N. Gribov and B. Pontecorvo, Neutrino astronomy and lepton charge, *Phys. Lett. B* **28**, 493 (1969).
- [138] S. Davidson, E. Nardi, and Y. Nir, Leptogenesis, *Phys. Rept.* **466**, 105 (2008), arXiv:0802.2962 [hep-ph].
- [139] W. Buchmuller, P. Di Bari, and M. Plumacher, Leptogenesis for pedestrians, *Annals Phys.* **315**, 305 (2005), arXiv:hep-ph/0401240.
- [140] W. Buchmuller, R. D. Peccei, and T. Yanagida, Leptogenesis as the origin of matter, *Ann. Rev. Nucl. Part. Sci.* **55**, 311 (2005), arXiv:hep-ph/0502169.
- [141] E. K. Akhmedov, V. A. Rubakov, and A. Y. Smirnov, Baryogenesis via neutrino oscillations, *Phys. Rev. Lett.* **81**, 1359 (1998), arXiv:hep-ph/9803255.
- [142] E. Nardi, Y. Nir, E. Roulet, and J. Racker, The Importance of flavor in leptogenesis, *JHEP* **01**, 164, arXiv:hep-ph/0601084.
- [143] P. H. Frampton, S. L. Glashow, and T. Yanagida, Cosmological sign of neutrino CP violation, *Phys. Lett. B* **548**, 119 (2002), arXiv:hep-ph/0208157.
- [144] W. Buchmuller, P. Di Bari, and M. Plumacher, Cosmic microwave background, matter - antimatter asymmetry and neutrino masses, *Nucl. Phys. B* **643**, 367 (2002), [Erratum: *Nucl. Phys. B* **793**, 362 (2008)], arXiv:hep-ph/0205349.
- [145] S. Pascoli, S. T. Petcov, and A. Riotto, Leptogenesis and Low Energy CP Violation in Neutrino Physics, *Nucl. Phys. B* **774**, 1 (2007), arXiv:hep-ph/0611338.
- [146] G. C. Branco, R. G. Felipe, and F. R. Joaquim, Leptonic CP Violation, *Rev. Mod. Phys.* **84**, 515 (2012), arXiv:1111.5332 [hep-ph].
- [147] A. De Rujula, M. B. Gavela, and P. Hernandez, Neutrino oscillation physics with a neutrino factory, *Nucl. Phys. B* **547**, 21 (1999), arXiv:hep-ph/9811390.
- [148] K. Abe *et al.* (T2K), The T2K Experiment, *Nucl. Instrum. Meth. A* **659**, 106 (2011), arXiv:1106.1238 [physics.ins-det].
- [149] T. Wachala, Recent Results on the CP Violation Search in the Accelerator Neutrino Oscillations, *Acta Phys. Polon. B* **48**, 1969 (2017).
- [150] M. A. Acero *et al.* (NOvA), Search for CP-violating Neutrino Non-Standard Interactions with the NOvA Experiment, (2024), arXiv:2403.07266 [hep-ex].
- [151] B. Brahma and A. Giri, Probing Dual NSI and CP Violation in DUNE and T2HK, (2023), arXiv:2306.05258 [hep-ph].